BIOLOGICAL RESEARCH CENTER OF THE HUNGARIAN ACADEMY OF SCIENCES, SZEGED

AND

DEPARTMENT OF PHARMACEUTICAL TECHNOLOGY
UNIVERSITY OF SZEGED

TARGETING PHARMACONS TO THE BRAIN VIA THE NASAL PATHWAY

Ph.D. thesis

Sándor Horvát

Supervisors:

Dr. Mária Deli, M.D., Ph.D.

Prof. István Erős, Ph.D., D.Sc.

2009.

CONTENTS

PUBLICATIONS RELATED TO THE SUBJECT OF THE THESIS

I. Wolburg H., Wolburg-Buchholz K.,·Sam K., Horvát S., Deli M.A., Mack A.F.
Epithelial and endothelial barriers in the olfactory region of the nasal cavity of the rat.
Histochemistry and Cell Biology; **130:** 127-140, 2008.
IF: 2.320 (2008)

II. Horvát S., Fehér A., Wolburg H., Sipos P., Veszelka S., Tóth A., Kis L., Kurunczi A., Balogh G., Kürti L., Erős I., Szabó-Révész P., Deli M.A.
Sodium hyaluronate as a mucoadhesive component in nasal formulation enhances delivery of molecules to brain tissue.
European Journal of Pharmaceutics and Biopharmaceutics; **72**: 252-259, 2009.
IF: 3.344 (2008)

III. Horvát S., Kis L., Dr. Szabóné Dr. Révész P., Dr. Erős I., Dr. Deli M.
Hatóanyagok agyba juttatása a nazális útvonalon keresztül**.**
Gyógyszerészet; **53**: 259-266, 2009.
IF: -

ABBREVIATIONS

ACTH	adrenocorticotropin
ANOVA	analysis of variance
AUC	area under the concentration-versus-time curve
AE	vehicle containing absorption enhancer
BA	bioavailability
BBB	blood–brain barrier
b. w.	body weight
CNS	central nervous system
CSF	cerebrospinal fluid
FD-4	fluorescein isothiocyanate-labeled dextran
GFAP	glial fibrillary acidic protein
HA	vehicle containing hyaluronan alone
ip.	intraperitoneal
iv.	intravenous
in.	intranasal
MA	vehicle containing mucoadhesive hyaluronan and absorption enhancer
MRP	multidrug resistance protein
OEC	olfactory ensheathing (glial) cells
PBS	phosphate-buffered saline solution
PFA	paraformaldehyde
PHS	physiological saline solution
SEM	standard error of mean
SF	sodium fluorescein
TBS	Tris-buffered saline solution
TJ	tight junctions
ZO	zonula occludens protein

1. INTRODUCTION

1.1. Drug targeting to the CNS

1.1.1. General considerations

The blood-brain barrier (BBB), a dynamic interface separating the brain from systemic circulation, is the major entry route for therapeutical compounds to the central nervous system (CNS). The estimated total length of human brain capillaries is 650 km, with a total surface area of 10 to 20 m^2 (Pardidge, 2002). Targeting of drugs to the CNS is still a difficult task to fulfill because the BBB prevents the influx of hydrophilic compounds with a molecular weight above 500 Da and ligands of efflux transporters from the systemic circulation into the brain. Hence, these barriers actively controlling cellular and molecular trafficking prevent the brain uptake of more than 98% of all potential neurotherapeutics (Pardridge, 2002). Therefore, successful treatment of CNS disorders like Parkinson's and Alzheimer's diseases, brain tumors, traumas or infections remained unsolved (Pardridge, 2005; Deli *et al.*, 2005). Due to specialised BBB functions only small lipophilic molecules, *e.g.* alcohol, nicotine, caffeine and cocaine, wich have limited therapeutic effects, are able to penetrate freely into the brain tissue by passive transport.

1.1.2. Drug transport and the BBB

The blood–brain barrier (BBB) is formed by brain endothelial cells lining the cerebral microvasculature. These cells are connected by tight junctions (TJ) (Fig. 1.).

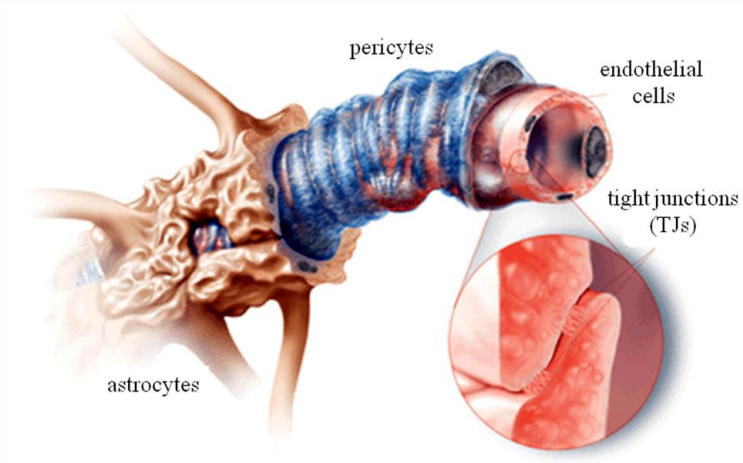

Fig. 1. Schematic drawing of brain microvessels. The BBB is a functional unit of endothelial cells, pericytes and astrocytes, a dynamic interface between blood and the CNS. (Miller, Science, 2002)

The TJs are built up by integral membrane proteins such as occludin, claudins and junctional adhesion molecules (JAM) which are connected to the actin cytoskeleton by linker proteins. Members of these cytoplasmic proteins are the zonula occludens proteins (ZO-1, ZO-2, ZO-3) and cingulin, among others (Krizbai and Deli, 2003). TJs restrict free paracellular flux of solutes and cells, this is the so called barrier function. The other specific function of TJs, the fence function creates cell polarity, which results in different protein, transporter, receptor compositions in brain endothelial membranes facing the blood or the brain (Abbott, 2006).

The brain endothelium has several unique receptors, transporters (Fig. 2.) and enzymes, which are localized in a polarized way in brain endothelial cells. The importance of transporters at the BBB is emphasized by the fact, that 11% of the brain endothelial genom codes genes of various transporters (Enerson and Drewes, 2006). These cells express a variety of transporters for nutrients, like glucose (glucose transporter-1 GLUT-1), neutral, acidic and basic amino acids (large neutral amino acid transporter LAT1), nucleosides (sodium-coupled nucleoside transporter CNT2), choline, vitamins, minerals, *etc.*, to feed neural cells (Abbott *et al.*, 2006) (Fig. 2. pathway 4.). Hence the BBB plays an important role in the homeostatic regulation of the brain microenvironment necessary for the stable and co-ordinated activity of neurons.

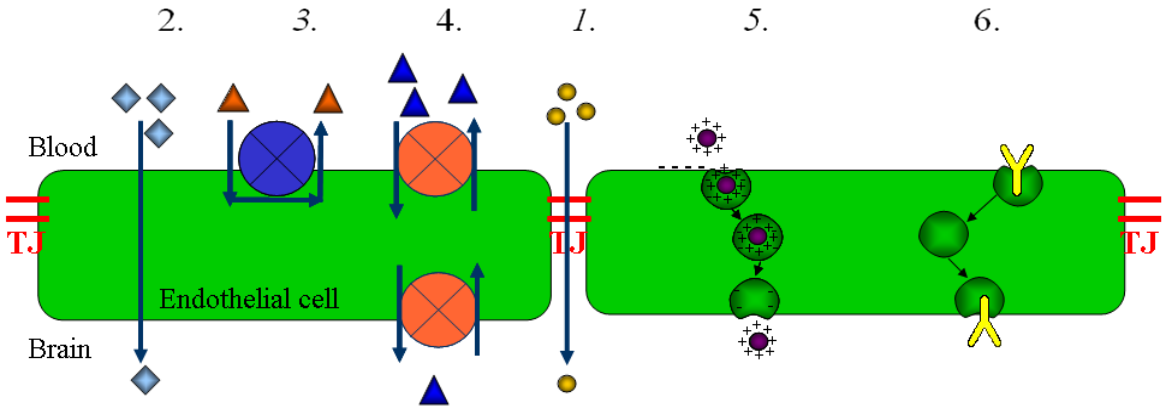

Fig. 2. Transport pathways at the BBB: 1. Paracellular aqueous pathway; 2. Transcellular lipophilic pathway; 3. Efflux transport; 4. Bidirectional carrier mediated transport; 5. Adsorptive transcytosis; 6. Receptor-mediated transcytosis

The BBB protects the CNS from fluctuations in plasma composition, and from circulating agents such as neurotransmitters and xenobiotics capable of disturbing neural function by efflux transporters (Fig. 2. pathway 3.). Some of these pumps belong to the family of ABC transporters, like P-glycoprotein (ABCB1), multidrug resistance proteins

MRP-1, -4, 5-, and -6 (ABCC1-6), and brain multidrug resistance protein (BMDP/ABCG2/BCRP), while others, *e.g.* organic anion-transporting polypeptide OATP2, organic acid transporters OAT1 and OAT3, or glutamate transporters EAAT1-3 do not (Pardridge, 2005).

These strictly regulated transport pathways, the low level of paracellular flux and non-specific transendothelial transport together with a concerted action of efflux pumps prevent the brain penetration of the great majority of possible therapeutical molecules.

1.2. Strategies to improve drug delivery to the CNS

In order to enhance the blood-brain transport and deliver drugs to the brain in an effective concentration, several approaches have been attempted. These methods include the modification of the drug molecules, or the manipulation of BBB. However, the increased transport of drugs to the CNS can be carried out not only by the modification of the BBB function or the drug molecule itself, but also via an alternative route by the selection of an application site circumventing the BBB.

1.2.1. Modification of the molecules

Because lipophilic molecules cross the BBB by free diffusion (Fig. 2. pathway 2.). Lipidisation, when molecules are made more lipophilic, is one of the most frequently used method to enhance brain penetration (Pardridge, 2002). Even large molecules, like proteins or nanoparticles have higher brain permeability when they are more cationic. Creating prodrugs by retrometabolic drug design is also an effective way of enhancing brain penetration of therapeutic compounds: using a sequential metabolism approach, the special bidirectional properties of the BBB can be exploited to smuggle the precursors of therapeutic compounds across the barrier and lock them inside the brain ready for sustained release of the active drugs (Bodor and Buchwald, 2002). Molecular trojan horses are therapeutic or diagnostic biomolecules bound to carriers, like endogenous peptides, modified proteins or peptidomimetic monoclonal antibodies, which exploit the transendothelial receptor-mediated pathway (Fig. 2., pathway 6.) at the BBB to target these molecules to brain (Pardridge, 2002; Pardridge, 2005).

1.2.2. Modification of the BBB functions

Hyperosmotic shock can reversibly open brain endothelial TJs (Deli, 2009). Ongoing multicenter clinical studies suggest that BBB disruption by intraarterial hyperosmotic mannitol can enhance the penetration of anticancer drugs and prolong survival in patients with malignant brain tumours (Muldoon, 2007). Vasoactive compounds, such as histamine, bradykinin, or leukotrienes are well-known mediators of brain oedema formation and increase BBB permeability. Some of these molecules have been investigated to increase brain penetration of active compounds (Deli, 2009).

Inhibition of efflux transporters at the BBB represent another possibility to enhance drug delivery. Therefore blockers of P-glycoprotein, the primary efflux pump in brain endothelial cells, are widely studied to increase the levels of therapeutic and diagnostic compounds in brain (Begley, 2004).

1.2.3. Alternative pathways to the brain

Because of the above mentioned therapeutical difficulties, circumvention of the BBB is used as a third strategy to enhance drug targeting to brain. One possibility is the direct injection of pharmacons to the brain tissue or to the cerebrospinal fluid (CSF), for the treatment of CNS infections and brain tumors. In tumor therapy medical sponges, minipumps can also be used. However these treatments are invasive and often painful. Utilization of alternative gateways to the brain, namely the nasal or ocular routes could represent another possibility.

1.3. The nasal pathway

In recent years nasal route for delivery of drugs to the brain via the olfactory region has received a lot of attention (Illum, 2000; Illum, 2003). This alternative pathway can be especially useful in the case of systemically acting drugs that are difficult to deliver via routes other than injection. The nasal route could be important for drugs that are used in crisis treatments, such as for pain, and for centrally acting drugs where the putative pathway from nose to brain might provide a faster and more specific therapeutic effect (Illum, 2002). Furthermore, the use of the nasal cavity for vaccination, especially against respiratory infections, is very promising, because it is possible to obtain, by the nasal route,

not only a systemic immune response, but also a local mucosal immune response that should provide a much higher level of protection against these diseases (Illum, 2002).

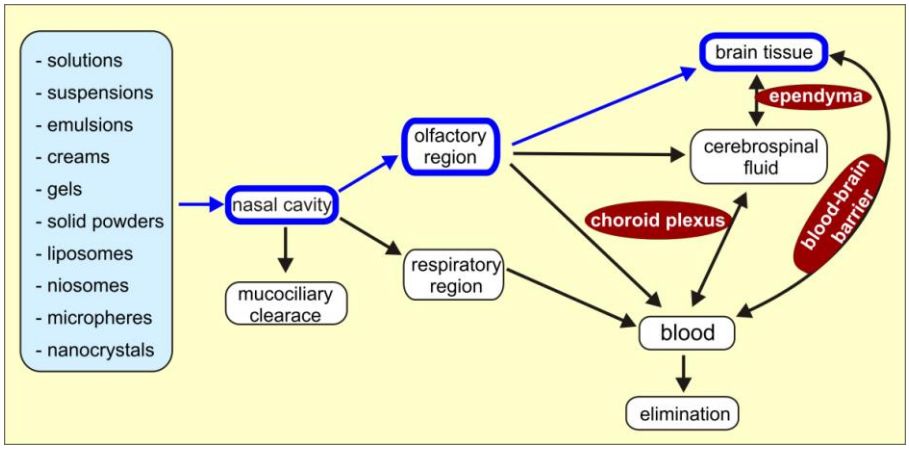

Fig 3. Pathways of nasal drug delivery

Intranasal delivery of drugs offers several advantageous properties. This method is non-invasive, essentially painless, can be easily and readily administered by the patient or a physician. Furthermore it ensures rapid absorption, the avoidance of first-pass metabolism in gut and liver and does not require sterile preparations (Zhang *et al*., 2004; Behl *et al*., 1998; Costantino *et al*., 2007).

ADVANTAGES	**DISADVANTAGES**
non-invasive	sensitivity of the nasal mucosa
no need for sterile formulation	irritation
painless	small volume of single dose: 25-200 µl
easy and simple application	quick elimination by mucociliary clearence
self administration	enzymic barrier
fast absorption, fast effect	upper respiratory tract diseases alter absorption
no first-pass elimination	
avoidance of gastrointestinal side effects	
applicable in case of nausea, vomiting and dysphagia	
lower risk of overdosing	
no decomposition of pharmacons at low gastric pH	
better compliance of patients	
direct pathway to the CNS	

Table 1. Advantages and disadvantages of nasal drug delivery

1.3.1. Anatomical and physiological characteristics of the olfactory region

The olfactory epithelium is an altered respiratory epithelium, capable of detecting odours due to the special anatomical structure. The olfactory region is positioned on the superior turbinate and opposite the nasal septum (Illum, 2000; Kürti *et al*., 2009). The surface of the olfactory region in animals with sensitive odour perception *e.g*. in dogs can be up to 170 cm^2. In man it covers an area of about 10 cm^2 from the total 150 cm^2 surface of the nasal cavity. Since the olfactory mucosa is positioned above the normal path of the air flow, odorants reach the sensitive receptors by diffusion. Sniffing enhances the diffusion process.

The olfactory epithelium consist of three cell types: the olfactory receptor cells, supporting epithelial cells and basal cells. Beneath the basement membrane is the lamina propria, which contains blood vessels, olfactory axon bundles (fila olfactoria), trigeminal nerve fibers and Bowman's glands, which secrete the mucus, that cover the epithelial surface. The Bowman's glands consist of an acinus, which is composed of acinar cells and duct cells, constitute the secretory duct going out through the olfactory epithelium. (Fig. 4.).

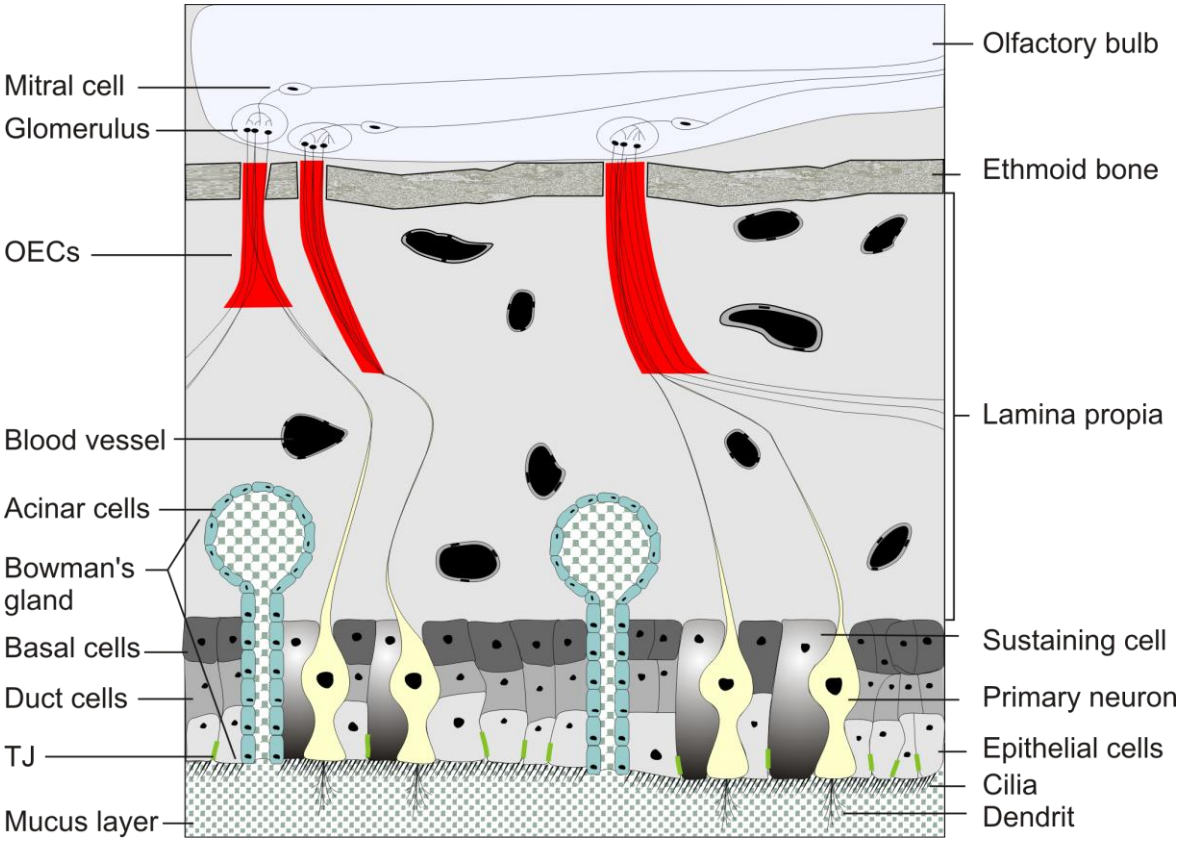

Fig. 4. Morphology of the olfactory region: various cell types.

In both the respiratory and olfactory regions the ciliated epithelial cells are closely connected on the apical surface by intercellular junctional complexes, which restrict cell and molecular trafficking across the epithelium.

The mucus layer, covering the epithelium consists of a low viscosity sol layer and a more viscous gel layer (Illum, 2000). The cilia move in a coordinated way to propel mucus across the epithelial surface towards the pharynx. This mechanism is called mucociliary clearence and results in the renewal of the mucus layer in every 15-20 minutes (Illum, 2003).

Olfactory sensory neurons are the only first order neurons whose cell bodies are located in a distal epithelium. Their dendritic processes are directly exposed to the external environment in the upper nasal passage while their unmyelinated axons, constituting fila olfactoria project through perforations in the cribriform plate of the ethmoid bone (Fig. 4., Fig. 5.) to synaptic glomeruli in the olfactory bulb. The fila olfactoria are wrapped in glial cells, so called olfactory ensheating cells (OECs) and surrounded by perineural cells. The perineural cell sheath is continuous with the meningeal sheath where the olfactory fila enter the olfactory bulb (Li *et al*., 2005). In the bulb the axons are synapsing with mitral cell dendrites forming the glomeruli. The supporting epithelial cells function as metabolic and physical support for the olfactory cells.

These unique anatomical and physiological properties of the olfactory region provide both extracellular and intracellular pathways into the CNS that bypass the BBB. The three major pathways are the olfactory nerve and the trigeminal nerve pathways, and paracellular mechanisms followed by uptake into the CSF (Fig. 5.) (Illum, 2000; Thorne *et al*., 2004).

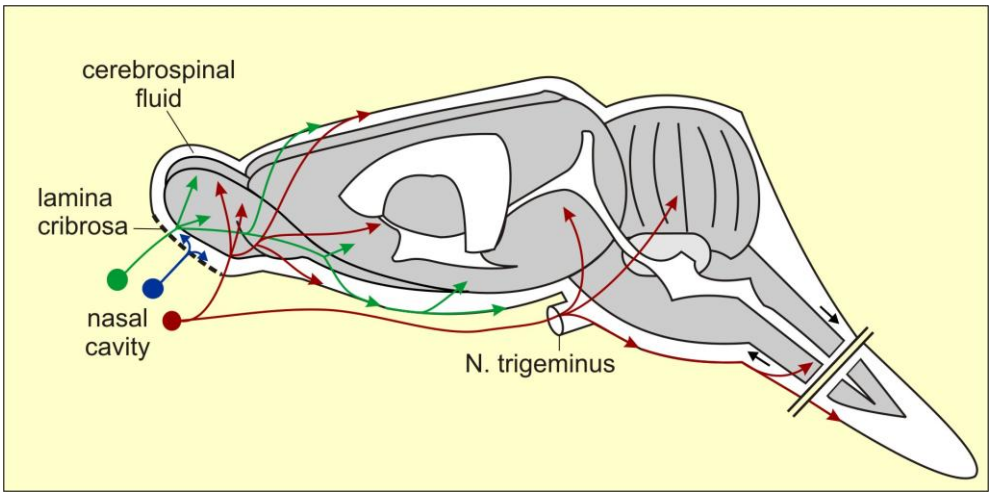

Fig 5. Transport pathways between the nasal cavity and the CNS. Possible transport routes via the olfactory and the trigeminal nerves, or in the CSF (Thorne et al., 2004)

1.3.2. Animal experiments and human data

It was realized early in the last century, that the olfactory region of the nose can be a major site for entry of viruses into the brain. It was shown that both poliomyelitis and vesicular stomatitis viruses can reach the brain via the olfactory neurons (Table 2.). Studies with tracer materials, potassium ferrocyanide, gold particles, aluminium lactate, wheat germ agglutinin-horsradish peroxidase also confirmed the usefulness of the nasal pathway in order to target molecules to the CNS (Illum, 2000). A large number of low molecular weight drugs and peptides, such as estradiol, progesterone, dihydroergotamine, cocaine, have been shown to reach the CSF, the olfactory bulb and in some cases other parts of the brain after nasal administration. Even large molecules, such as the proteins nerve growth factor, insulin-like growth factor and fibroblast growth factor could be transported to the CNS (Table 2.).

Experimental material nasally administered	**Animal model**	**Affected brain region /measurement of effect**	**Authors, year**
Microorganisms			
neurotropic poliomyelitis virus	Rhesus monkey	olfactory bulb, CSF	Landsteiner and Levaditi, 1910
vesicular stomatitis virus	mouse	olfactory bulb, whole brain	Sabin and Olitsky 1937
Tracer materials			
potassium ferrocyanide, iron ammonium citrate	rabbit	whole brain	Faber, 1937
gold particles	squirrel monkey	olfactory bulb	De Lorenzo, 1970
aluminium-lactate	rabbit	olfactory bulb, cortex	Perl and Good, 1987
fluorescein	rat	striatum	Bagger and Bechgaard, 2003
Peptides, proteins, pharmacons			
wheat germ agglutinin–horseradish peroxidase	rat	olfactory cortex, midbrain, pons	Shipley, 1985
vazopressin	rat	biological effect	Morimoto *et al*., 1990
nerve growth factor	rat	olfactory bulb, cerebellum, brain stem	Frey *et al*., 1995
diazepam	rat	behind the olfactory bulb	Gizurarson *et al*., 1996
dihydroergotamine	rat	olfactory bulb	Wang *et al*., 1998
dopamine	mouse	cerebrum	Dahlin *et al*., 2000
methotrexate	rat	CSF	Wang *et al*., 2003

estradiol, progesterone	rat	CSF	van den Berg *et al*., 2004
insulin-like growth factor	rat	olfactory bulb, frontal cortex, brain stem	Thorne *et al*., 2004
fibroblast growth factor	rat	hippocampus, striatum	Wang *et al*., 2008

Table 2. Experimental materials nasally targeted to brain: animal studies

Most of the studies evaulating nose to brain delivery of drugs in man measured indirectly the pharmacological effects of drugs on the CNS (Table 3.). Nasally administered arginine-vasopressin, cholecystokinin-8 and insulin increased performances in behavioral tests, like auditory attention task and Stroop test, and enhanced thinking in volunteers (Illum, 2004). Adrenocorticotropin 4-10 (ACTH 4-10) administered nasally twice daily for six weeks, reduced body fat and body weight without significant changes in serum concentration of the peptide.

Experimental material nasally administered	**Number of volunteers**	**Experimental method**	**Authors, year**
arginine-vasopressin	15	behavioral study	Pietrowsky *et al*., 1996
cholecystokinin-8	20	behavioral study	Pietrowsky *et al*., 1996
insulin	18	behavioral study	Pietrowsky *et al*., 1996
99mTc-DTPA-hyaluronidase	2	γ-scintigraphy	Okuyama, 1997
angiotensin II	12	blood pressure measurement	Derad *et al*., 1998
ACTH 4-10	54	behavioral study	Smolnik *et al*., 1999
insulin	8	CSF study	Fehm *et al*., 2000
insulin	12	behavioral study	Kern *et al*., 2001
diazepam	8	EEG-test	Lindhardt *et al*., 2001
apomorphine	5	CSF study	Quay, 2001
insulin, melanocortin, vasopressin	36	CSF study	Born *et al*., 2002
melatonin/hydroxycobalamin	8	CSF study	Merkus, 2003

Table 3. Experimental material nasally targeted to brain: human studies

There are also available data on the direct mesurement of nose to brain transport in man (Table 3.). In an anosmic female volunteer a significant rise in cerebral radioactivity

was observed after introduction of a radiotracer in the form of nasal spray (Okuyama, 1997). In an other study nasal administration of melanocortin 4-10, vasopressin and insulin resulted of a significant increase of CSF concentration at 80 minutes after treatment (Born *et al*., 2002). All these data confirm the likely existence of the nasal route to the CNS in man.

The pathways employed for delivery of a particular drug from the nose to the brain is highly dependent on various factors, such as the existence of specific receptors on the olfactory neurons, the lipophilicity and the molecular weight of the drug (Illum, 2000). It is likely that drugs may use more then one pathway.

1.3.3 Formulation factors influencing drug delivery via the nasal pathway

During the formulation of a dosage form intended for intranasal application several aspects should be taken into consideration (Ugwoke *et al*., 2005). The olfactory region in man is situated in the upper part of the nasal cavity, an area that is difficult to reach with presently available nasal spray or powder devices. Furthermore the nasally administered drugs will normally be cleared rapidly from the nasal cavity into the gastrointestinal tract by the mucociliary clearance system (Fig. 3., Illum, 2003). Other important factors limiting the nasal absorption of large molecular weight or polar drugs are the low membrane permeability and the interepithelial junctional complexes, which hinders the trans- and paracellular transport of polar drugs (Khafagy, 2007). Moreover, the nasal mucosa has a metabolic capacity as well, which can contribute to the low transport of peptides and proteins across the nasal membrane (Zhang *et al*., 2004; Costantino *et al*., 2007; Ugwoke *et al*., 2005). Because of these reasons application of (i) mucoadhesive agents to increase residence time of formulations on the nasal mucosa and (ii) absorption enhancers to elevate drug transport across the nasal mucosa is crucial in nasal vehicles.

We chose for our studies sodium hyalutonate, as a mucoadhesive component. It is the sodium salt of hyaluronic acid, a naturally occurring linear polysaccharide composed of alternating disaccharide units of *N*-acetyl-D-glucosamine and D-glucuronic acid (Fig. 6., Liao *et al*., 2005).

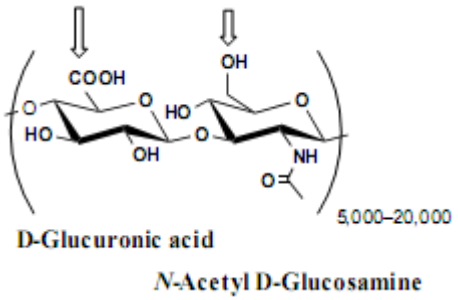

Fig. 6. Chemical structure of hyaluronate (Vercruysse and Prestwich, 1998)

Hyaluronic acid, a non-sulfated glycosaminoglycan, can be found in the extracellular tissue matrix of vertebrates, including connective tissue, synovial fluids, vitreous humour and aqueous humour (Jiang *et al*., 2007). It plays a critical role as a signaling molecule in cell motility, cell differentiation, and wound healing. This natural anionic polysaccharide has an excellent mucoadhesive capacity (Liao *et al*., 2005; Ludwig, 2005) and many important applications in formulation of bioadhesive drug delivery systems (Vercruysse and Prestwich, 1998). Beside its mucoadhesive properties it was found that this biopolymer may enhance the absorption of drugs and proteins via mucosal tissues (Ludwig, 2005; Cho *et al*., 2003; Lim *et al*., 2000). While hyaluronan is used in diverse drug delivery systems e.g. ophthalmic, pulmonary and vaginal (Liao *et al*., 2005; Ludwig, 2005, Bonferoni *et al*., 2006), it has not been widely exploited for nasal drug delivery to the nervous system.

It is possible to greatly improve the nasal absorption of polar drugs by administering them in combination with an absorption enhancer that promotes the transport of the drug across the nasal membrane (Illum, 2002). Chitosans and other positively charged polymers, cyclodextrins, lectins, phospholipids and lipids have been applied in novel nasal delivery systems (Lehr, 2000; Illum, 2002). As an absorption enhancer polyethoxylated 40 hydrogenated castor oil (Cremophor RH40), a non-ionic solubilizing and emulsifying agent, was selected for our experiments. This surfactant can be used to increase bioavailability of drugs by solubilizing of poorly soluble compounds and increasing cell membrane fluidity. Furthermore, Cremophors have been shown to inhibit P-glycoprotein activity, therefore, they increase the bioavailability of drugs which are known substrates of this efflux transporter (Narang *et al*., 2007; Regea *et al*., 2002; Pouton, 2006; Takano *et al*., 2006).

Altough a range of novel nasal products for systemic delivery of therapeutics has reached the market already (Illum, 2002; Kürti *et al*., 2009), there is still no drug exploiting the nasal route to treat CNS diseases. Development of nasal delivery systems that enable

rapid and efficient concentration of drugs in the brain is a new and important field of investigation.

1.4 Aims

Considering the above mentioned aspects of nasal drug targeting to the brain, the importance of the permeability properties of the olfactory region, and the role of nasal vehicles in drug delivery, the main aims of our experiments were the following:

(1) to reveal the protein composition of the junctional complexes of the olfactory region by immunohistochemistry,
(2) to characterize the permeability of blood vessels in different parts of the olfactory system from the nasal cavity to the CNS,
(3) to formulate and characterize carrier systems for nasal delivery containig bioadhesive and/or absorption enhancer components,
(4) to measure plasma and brain pharmacokinetics and bioavailability using different vehicles and fluorescein isothiocyanate-labeled dextran with an average molecular weight of 4.4 kDa (FD-4) as a test molecule in rats,
(5) to test the acute toxicity of nasal vehicles on the olfactory system.

2. MATERIALS AND METHODS

2.1. Materials

All reagents, including FITC-labeled dextran (FD-4; Mw = 4.4 kDa) were purchased from Sigma-Aldrich Chemical Co. (MO, USA), unless otherwise indicated. Polyethoxylated 40 hydrogenated castor oil (Cremophor RH40) was obtained from BASF (Germany). Sodium hyaluronate (Mw = 1400 kDa) was obtained as a gift from Gedeon Richter Ltd. (Hungary). All other materials were of reagent grade.

2.2. Antibodies and immunohistochemistry

The following antibodies were used to detect specific tight junction proteins: polyclonal rabbit anti-claudin-1, polyclonal rabbit anti-claudin-3, polyclonal rabbit anti-occludin, monoclonal mouse anti-ZO-1 and polyclonal rabbit anti-ZO-1 (Zymed, San Francisco, USA) polyclonal rabbit anti-claudin-5 (Liebner *et al*., 2000), polyclonal rabbit anti-claudin-19 (kindly provided by Mikio Furuse, Kobe, Japan), polyclonal rabbit anti-ZO-2 (Cell Systems, Remagen, Germany), polyclonal rabbit anti-connexin-43. All antisera were used in a dilution of 1:100. The secondary goat anti-mouse and anti-rabbit antibodies labelled with cyanin-derivative dye Cy3 or Cy2 were purchased from Dianova (Hamburg, Germany). For controls, the primary antibody was omitted. Nuclei were stained with Sytox (green; 1:10,000) or Topro (blue; 1:10,000), both Molecular Probes/Invitrogen, Karlsruhe, Germany.

Untreated rats were anesthetized and transcardially perfused with 4% paraformaldehyde (PFA). Olfactory epithelium was dissected out and postfixed in 4% PFA in phosphate-buffered saline solution (PBS, pH = 7.4) overnight. Subsequently, the tissue was embedded in paraffin and sectioned at 3 μm using a microtome (HM355SS; Micron international, Walldorf, Germany). Sections were placed on Super Frost Plus slides (Micron international, Walldorf, Germany), dewaxed, and rehydrated by descending alcohol concentrations to aqua dest. For antigen retrieval, they were heated in a steamer in citrate buffer pH 6.0 for 4 min, and finally coated in Tris-buffered saline solution (TBS). To avoid unspecific staining, the sections were blocked by incubation with 5% (w/v) skimmed milk, 0.3% (w/v) Triton X-100 (Serva, Heidelberg, Germany) and 0.4% (w/v) NaN_3 in TBS for 30 min. Primary antibodies diluted in the same solution were applied

overnight at 4°C. After three washes in TBS for 10 min, sections were incubated for 45 min with the secondary antibody at room temperature. Following washes in TBS, sections were mounted in Mowiol. Sections were analyzed with a confocal laser scanning microscope (LSM510 META with an Axioplan 2 microscope stand, Zeiss, Göttingen/Jena, Germany) using lasers at 488, 546, and 633 nm for excitation with appropriate filter sets. Images were processed using Adobe Photoshop (version 7.0, Adobe, Mountain View, USA).

2.3. Permeability studies

Vascular permeability of the olfactory system was demonstrated by extravasation of the marker fluorescein (MW 376 Da) and Evan's blue that binds serum albumin (MW 67 kDa). Under Tribromoethanol (1.25%, 10 ml/kg body weight) anesthesia rats were given a solution of both dyes (2%, 5 ml/kg b. w.) in an injection into the tail vein. After 30 min, the animals were perfused transcardially with 50 ml phosphate-buffered saline for 5 min. The heads were dissected and macroscopic pictures were taken from the head sagittal sections.

In case when the permeability of the blood vessels was tested by means of electron microscopy, 1% lanthanum nitrate was added to the fixative, which was followed by transcardial perfusion (see for electron microscopy).

2.4. Preparation of dosing solutions

Cremophor RH40 was dissolved in physiological saline solution (PhS; 0.9% w/v sodium chloride in sterile distilled water). In case of sodium hyaluronate-containing samples the mucoadhesive polymer was added in small amounts to the solution. In order to ensure the complete solvation of polymers, samples were rehomogenized after 24 h. The FD-4 was dissolved in the prepared vehicles. The concentration of the test molecule was 1 mg/ml for intranasal and 8 mg/ml for intravenous administration. The compositions of the dosing solutions are shown in Table 4.

Vehicle	Physiological saline	Sodium hyaluronate	Cremophor RH40
PhS	100.0%	-	-
AE	90.0%	-	10%
HA	98.5%	1.5%	-
MA	88.5%	1.5%	10%

Table 4. Compositions of the dosing solutions (in weight percentage)

2.5. Rheological measurements

Rheological measurements were carried out with a Rheostress 1 Haake instrument. A cone-plate measuring device was used in which the cone angle was 1º, and the thickness of the sample was 0.048 mm in the middle of the device. The flow and viscosity curves of the samples were determined by changing the shear rate between 0.01 and 100 s^{-1} at 37ºC.

2.6. *In vitro* drug release studies

In case of samples with 1 mg/ml FD-4 content, *in vitro* drug release experiments were performed as well. The dissolution studies were carried out using ointment cells and small volume dissolution vessels in a Hanson SR8-plus dissolution apparatus (Chatsworth, CA, USA). Samples, 0.4 g each, were placed as donor phase on the Porafil membrane filter (pore diameter 0.45 μm). The effective diffusion surface area was 1.767 cm^2. PBS (pH = 7.4, 100 ml) was used as dissolution medium at a temperature of 37ºC and a paddle speed of 50 rpm. Samples (3 ml each) were taken and immediately replaced with fresh dissolution medium at 15, 30, 60, 120, 180, 240, 300, 360, 420 and 480 min, and further analyzed by spectrofluorometry. Six parallel measurements were performed in case of each dosing solution. Dissolution profiles were compared by using difference factor f1 and similarity factor f2. For two similar preparations, the value of f1 must be between 0 and 15 and that of f2 must be in the range of 50–100. The factors can be calculated according to the following equations: (Shah, *et al*., 1998; Guidance for Industry, 1997; O'Hara, *et al*., 1998),

$$f_1 = \left\{ \left[\sum_{t=1}^{n} \left| R_t - T_t \right| \right] / \left[\sum_{t=1}^{n} R_t \right] \right\} x100 \qquad \text{Eq. (1)}$$

$$f_2 = 50\ x \log \left\{ \left[1 + \left(1/n \sum_{t=1}^{n} \left(R_t - T_t \right)^2 \right) \right]^{-0.5} x100 \right\} \qquad \text{Eq. (2)}$$

where n is the number of time points, R is the dissolution value of the reference batch at time t, and T is the dissolution value of the test batch at time t.

2.7. Animal experiments

Male Wistar rats (316 ± 48 g, 3-month-old) were used for all the studies. The animals were obtained from the animal facility of the Biological Research Center, Szeged, kept under standard conditions, and given tap water and rat chow *ad libitum*. The experiments performed conform to European Communities ‘‘Council directive for the care and use of laboratory animals’’ and were approved by local authorities (XVI./03835/001/2006).

2.7.1. Treatments

Nasal administration was performed as follows: The rats were anesthetized ip. with tribromoethanol solution and they were placed in supine position. An average of 40 µl solution was then administrated by micropipette positioned 5 mm deep into the right naris to achieve the longest possible residency time of the vehicle in the nasal cavity. In case of intravenous treatment 500 µl solution was injected into the tail vein of anesthetized animals. There were five treatment groups as shown in Table 5., and five different time points, 30, 60, 120, 240 and 480 min, during the experiments.

Vehicle	Treatment	n	V_{FD-4}	C_{FD-4}	m_{FD-4}
PhS	intravenous	4	500 µl	8 mg/ml	4000 µg
PhS	intranasal	4	40 µl	1 mg/ml	40 µg
AE	intranasal	4	40 µl	1 mg/ml	40 µg
HA	intranasal	4	40 µl	1 mg/ml	40 µg
MA	intranasal	4	40 µl	1 mg/ml	40 µg

Table 5. The composition of the experimental groups. n, number of animals/group; V, volume of the dosing solution given for treatment; C, concentration of FD-4 in dosing solutions; m, quantity of FD-4 given in dosing solutions/animal; PhS, physiological saline solution; AE, vehicle containing absorption enhancer Cremophor RH40; HA, vehicle containing hyaluronan alone; MA, vehicle containing mucoadhesive hyaluronan and absorption enhancer Cremophor RH40.

2.7.2. Collection of plasma and brain samples for the measurement of FD-4 levels

In deep anesthesia 30, 60, 120, 240, 480 min after the treatments, 200 µl blood was taken by cardiac puncture into heparinized tubes from all four rats in each treatment group and at each time point, then the animals were transcardially perfused (100 ml PBS, pH = 7.4). The brains were removed and 10 brain regions including the olfactory bulb, frontal and parietal cortex from the left and the right side, the hippocampus, the midbrain, the pons and the cerebellum were excised. The weight of the brain samples was measured. Blood samples were immediately centrifuged (10 min, 3000g), and plasma samples were transferred to new tubes. All samples were kept frozen until further investigations.

2.8. Determination of FD-4 concentration of samples

Brain samples were homogenized with 1 ml of 7.5% w/v trichloroacetic acid solution in Potter–Elvehjem tissue grinder. Homogenized samples were centrifuged at 9500g for 10 min at 4ºC. 800 µl of supernatant was neutralized by addition of 2N NaOH solution. In case of samples obtained from the *in vitro* drug release experiment, the above-mentioned pre-treatment was not required. The FD-4 content of samples was determined by a PTI spectrofluorometer (Photon Technology International Inc., South Brunswick, NJ, USA) at excitation wavelength of 492.5 nm and emission wavelength of 514.5 nm. The sensitivity of the measurement was 1 ng/ml FD-4 in the samples. Linearity of the measurement of FD-4 was $r^2 \geq 0.9986$, while the precision was found to be RSD ≤ 9.19% across all the concentration ranges used in the study.

2.9. Electron microscopy

Rats were transcardially perfused with 2.5% glutaraldehyde (Paesel-Lorei, Frankfurt, Germany) buffered in 0.1 M cacodylate buffer (pH 7.4). Thereafter, the olfactory tissue was dissected out and postfixed in the identical fixative for additional 4 h, and then stored in cacodylate until further processed. The tissues (cerebral cortex, olfactory bulb, nasal mucosa) were postfixed in 1% OsO_4 in 0.1 M cacodylate buffer and then dehydrated in an ethanol series (50, 70, 96, 100%). The 70% ethanol was saturated with uranyl acetate for contrast enhancement. Dehydration was completed in propylene oxide. The specimens were embedded in Araldite (Serva, Heidelberg, Germany). Ultrathin sections were produced on a FCR Reichert Ultracut ultramicrotome (Leica, Bensheim, Germany), mounted on pioloform-coated copper grids, contrasted with lead citrate and analyzed and documented with an EM10A electron microscope (Carl Zeiss, Oberkochen, Germany).

2.10. Statistical analysis

All data presented are means ± SEM or SD The values were compared using GraphPad Prism software (GraphPad Software Inc., San Diego, CA, USA). The analysis of variance was followed by Newman–Keuls multiple comparison test. Changes were considered statistically significant at $P < 0.05$.

3. RESULTS

3.1. Immunostainings of junctional proteins in the olfactory system

ZO-1

Investigating the classical TJ protein ZO-1, we found positive reactions to all types of TJs in the olfactory epithelium and the lamina propria: In the apical regions of the olfactory epithelium, between the acinar cells and duct cells of Bowman's glands, between endothelial cells of the vessels, perineural cells around the olfactory fila, and between olfactory ensheathing cells (OECs) (Figs. 7., 8.).

ZO-2

Apical junctions of the olfactory epithelium (between supporting cells and the dendrites of the sensory cells) were heavily labelled by antibodies for the TJ-associated protein ZO-2, as were the apical junctions of the acinar cells of the Bowman's gland, and endothelial cells (Fig. 7.). Here we detected a strong co-labeling with ZO-1. The TJs of perineural cells and OECs, positive for ZO-1, were devoid of ZO-2. Interestingly, the basal region of the olfactory epithelium was clearly stained with the anti-ZO-2-antibody, but not with the anti-ZO-1 antibody (Fig. 7. A).

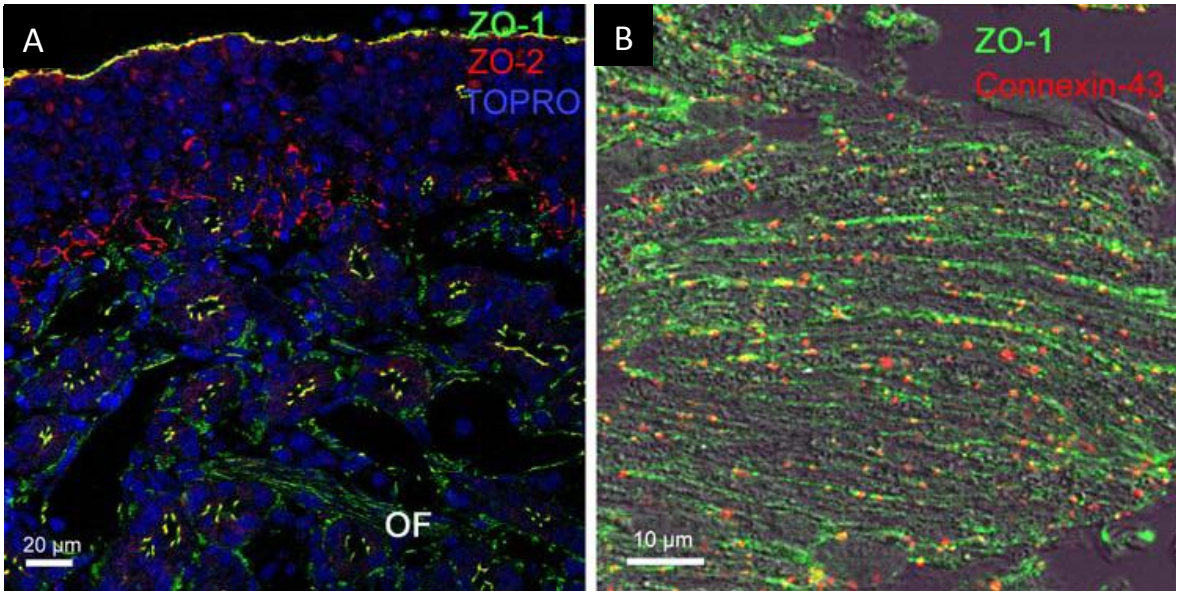

Fig. 7. A: *ZO-1(green) and ZO-2 (red) molecules were co-localized in the olfactory and the Bowman's gland epithelial cells (merged as yellow). The basal cells in the olfactory epithelium were stained selectively by anti-ZO-2 antibody. The OECs in the olfactory fila did not express ZO-2, but ZO-1.* B: *ZO-1 (green) and connexin 43 (red) immunostaining show gap junctions and TJs interconnecting the OECs within the olfactory fila. Yellow points mark an overlay of Cx43- and ZO-1-immunoreactivities.*

Connexin-43

Previously, the gap junction protein connexin-43 had been detected on many cells in the olfactory system (Rash et al. 2005). Connexin-43 co-localized with the TJs between the OECs: spots double labelled for connexin-43 and ZO-1 were found OECs (Fig. 7.).

Claudin-1

We tested the olfactory tissues for the presence of claudin-1. The apical TJs of the olfactory epithelium between the supporting cells and the sensory cell dendrites, and perineural cells around the olfactory fila stained positive for claudin-1-antibodies. The OECs were devoid of any claudin-1 staining (Fig. 8. A, B).

Claudin-3

In the olfactory mucosa, a specific signal could be detected in the olfactory epithelium and in the Bowman's glands (Fig. 8. C).In contrast, the endothelial cells within the olfactory lamina propria were negative for claudin-3. OECs and the perineural cells were immunonegative for claudin-3 (Fig. 8. C) as well.

Claudin-5

The occurrence of the endothelial TJ protein claudin-5 was confirmed in the blood vessels of the olfactory lamina propria. However, the immunoreactivity was rather weak, likely due to the extremely thin walls of the blood vessels in this tissue and rare occurrence of these TJs in thin sections (Fig. 8. D). Claudin-5 could also be detected both in the apical TJs of the olfactory epithelium and in the OECs of the olfactory fila (Fig. 8. D).

Claudin-19

The TJ molecule claudin-19 characteristic for Schwann cells was tested for its presence in the olfactory system. Claudin-19 immunoreactivity was found in the apical region of the olfactory epithelium showing TJs between supporting cells and the dendrites of the sensory olfactory neurons, but not in OECs (Fig. 8. E).

Occludin

Occludin was the first integral membrane protein of TJs detected. For the olfactory system, we confirmed the unambiguously distinct staining of apical olfactory TJs (Fig. 8. F). For the first time we showed occludin in the fila olfactoria between the OECs (Fig. 8. F). Endothelial TJs were positively stained as well. Interestingly, in the acinar cells of the Bowman's glands, occludin-specific staining was not restricted to the apical region but spread over most of the cell surface, although the TJs proper are restricted to the most apical region of the cells shown by anti-ZO-1 staining (Fig. 8. F).

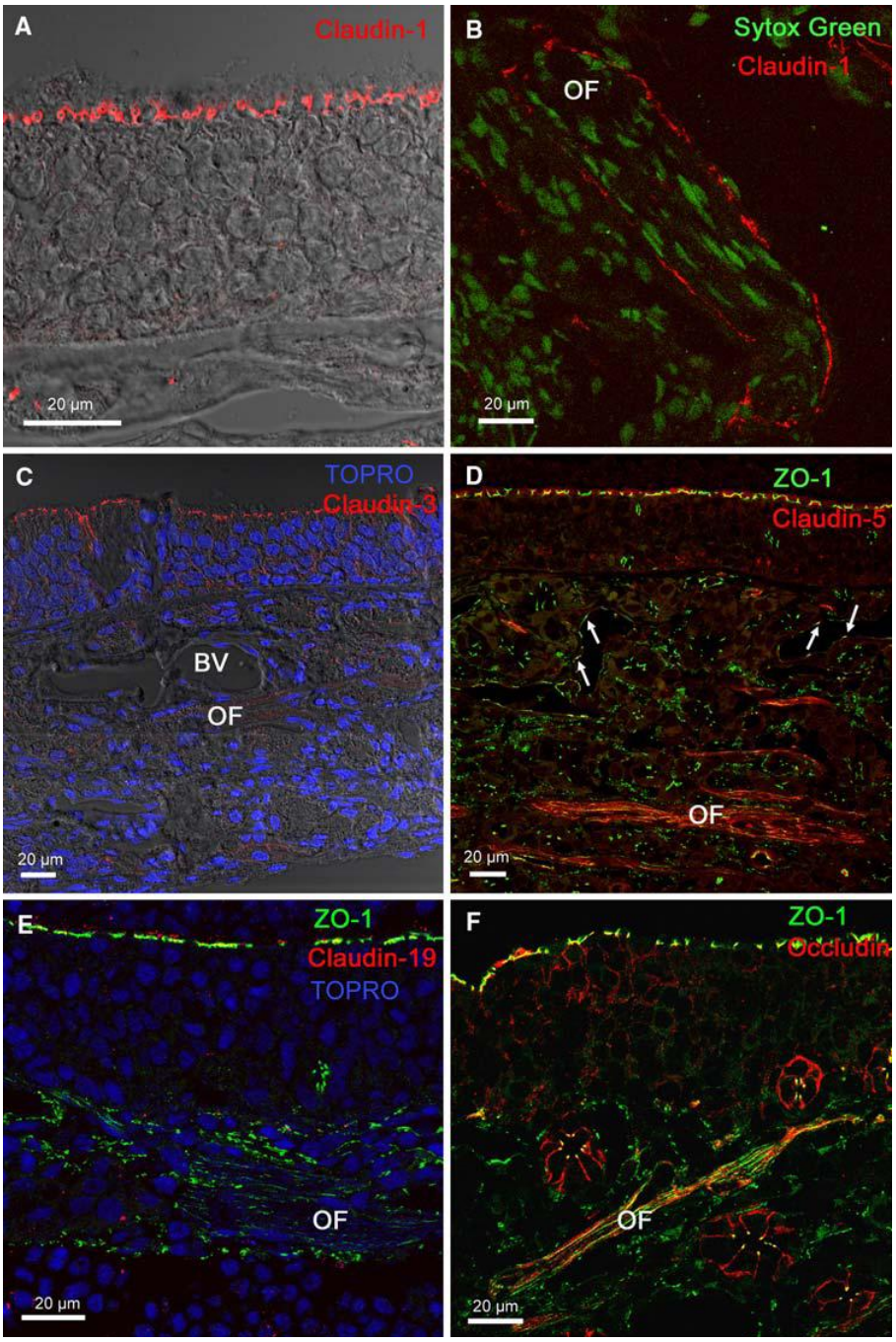

Fig 8. Immunohistochemical stainings of the peripheral olfactory system: olfactory epithelium and lamina propria with olfactory fila (OF). ***Claudin-1*** *staining (red) of the apical TJs between supporting cells and dendrites of the sensory epithelial cells (A), and perineural cells (B). The OECs were immunonegative for claudin- 1.* ***Claudin-3*** *(red) stains the apical TJs in the olfactory epithelium and the Bowman's gland epithelial cells. Importantly, the blood vessel (BV) endothelial cells were not immunoreactive for claudin-3 (C). Whereas the* ***claudin-5*** *(red) immunoreactivity was difficult to detect in vascular endothelial cells (arrows), it could easily be found in the olfactory fila. In addition, the apical TJs of the olfactory epithelium were also positively stained with the anticlaudin-5 antibody, seen as overlapping staining with ZO-1 green) (D). Apical TJs of the olfactory epithelium were immunoreactive against* ***claudin-19*** *(red) (E), however olfactory ensheathing cells were negative for claudin-19. ZO-1 (green) and* ***occludin*** *(red) molecules are colocalized in the olfactory and the Bowman's gland epithelial cells (merged as yellow). In addition, occludin stains the entire surface of Bowman's glandular cells, and, more weakly, the basolateral membranes of the olfactory epithelium (F).*

3.2. Permeability studies

In order to test the permeability of blood vessels in the olfactory system, we injected Evan's blue and fluorescein dyes intravenously. The marker dyes leaked out of blood vessels in the entire olfactory system. Evan's blue and fluorescein together stained the tissue green, whereas the brain remained unstained (Fig. 9.).

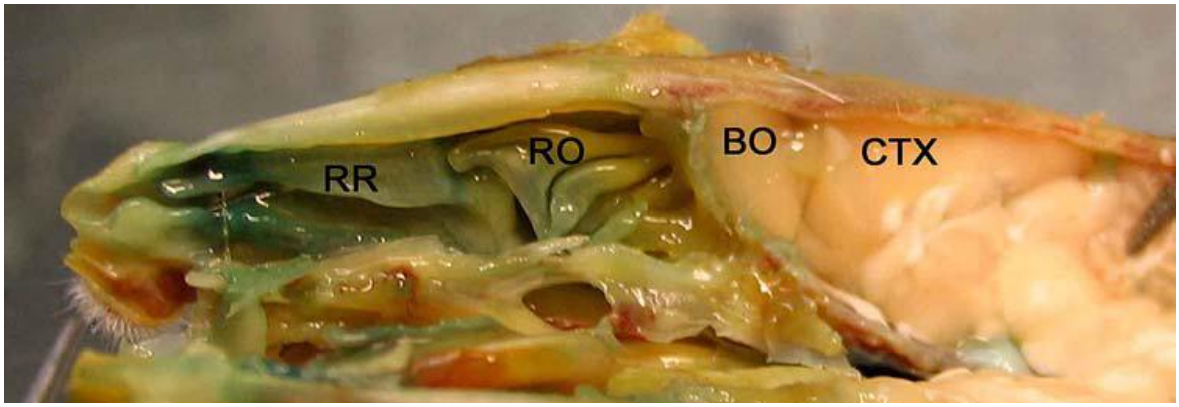

Fig 9. Macroscopical aspect of the rat brain after injection of Evan's blue and fluorescein into the tail vein. As can clearly be seen, both the respiratory (RR) as well as the olfactory region (OR) of the nasal cavity were stained green-blue, directly showing the high permeability of the blood vessels in this region of the olfactory system. In contrast, the brain (cortex, CTX) including the olfactory bulb (BO) remained unstained.

In a second permeability experiment rats were transcardially perfused with glutaraldehyde containing 1% lanthanum nitrate, a small molecular weight paracellular permeability marker. Lanthanum nitrate, could easily be detected in the electron microscope as a black precipitate and allowed us to distinguish between tracer penetrating the interendothelial cleft or being transported through the endothelial cells via endocytosis. As expected, the blood vessels within both the cerebral cortex (Fig. 10. A, B) and the olfactory bulb (Fig. 10. C, D) were tight for lanthanum. The tracer diffused only a small distance between the cells, approximately of 0.5–1 μm, and then abruptly stopped where the TJ obstructed the way. The subendothelial space, in particular the basal lamina, was devoid of any tracer particles (Fig. 10. A-D). In clear contrast, the blood vessels of the olfactory lamina propria of the same animals were leaky: the lanthanum had travelled through the entire interendothelial cleft and labelled the subendothelial space (Fig. 10. E). Both the subendothelial basal lamina and the basal lamina around the olfactory fila were labelled, demonstrating that the TJs were not able to obstruct the paracellular passage between the endothelial cells. The lanthanum that had leaked through not only labelled the subendothelial basal lamina, but also the basal lamina covering the OECs (see large arrow in Fig. 10. F).

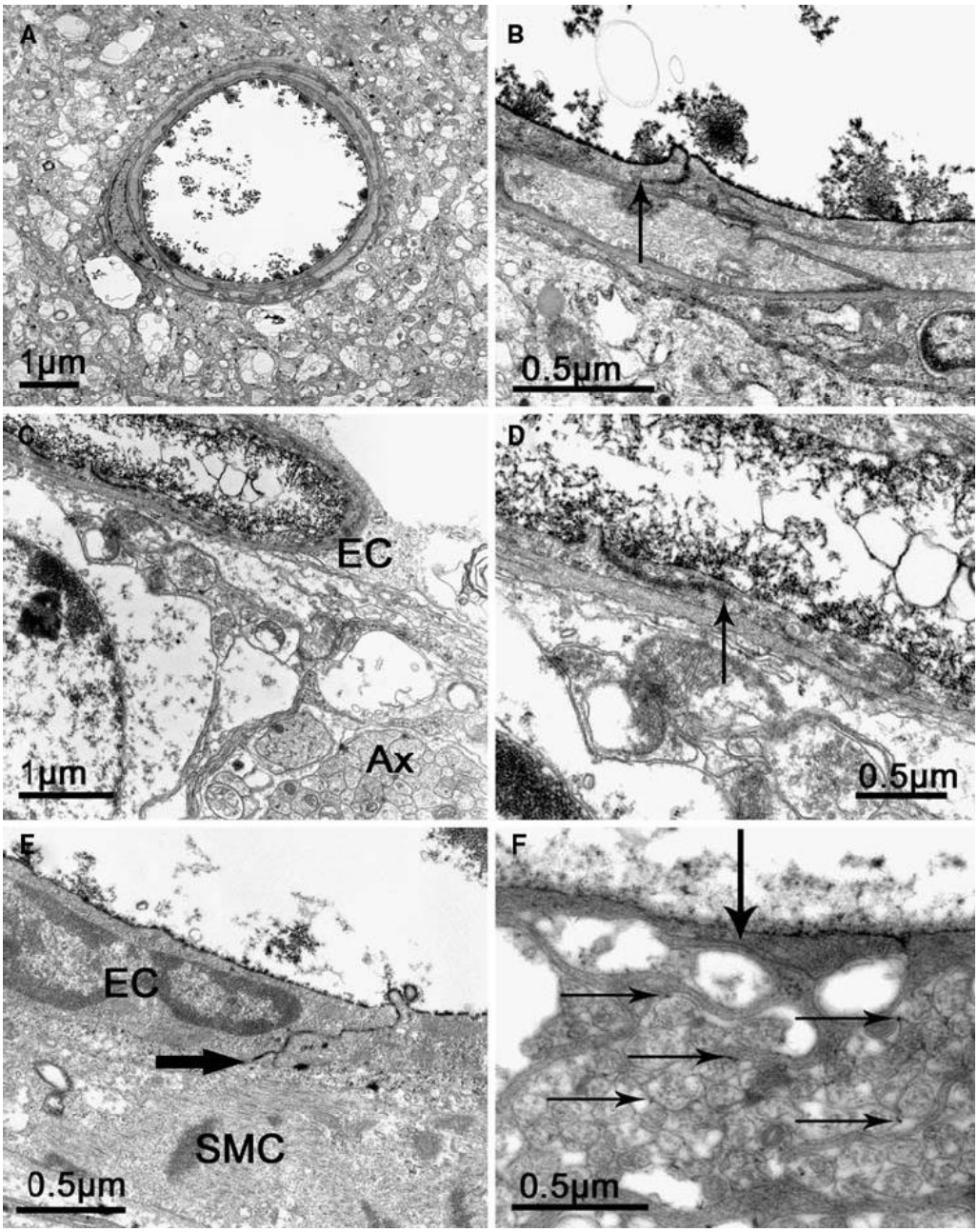

Fig. 10. A, B: Lanthanum labelling after transcardial perfusion of lanthanum nitrate together with the fixative. Analysis of the lanthanum distribution in cortical vessels at low (A) and higher (B) magnification. The arrow in B shows the stop of lanthanum penetrating the interendothelial cleft: the subendothelial space was unstained and clean of lanthanum.
C, D: The same experiment as shown in A, B in the olfactory bulb. In C, olfactory axons (Ax) running into the olfactory bulb were located near a blood vessel. This vessel is tight as shown by restriction of lanthanum penetration within the interendothelial cleft (arrow in D).
E: Analysis of the lanthanum distribution in the lamina propria of the olfactory system. The interendothelial cleft was open indicated by lanthanum deposits down to the subendothelial space (arrow). EC-endothelial cell, SMC-smooth muscle cell.
F Analysis of the lanthanum distribution in an olfactory filum. The basal lamina surrounding the filum (top) was labelled by numerous lanthanum deposits. The large arrow points to a TJ interconnecting two processes of an olfactory ensheathing cell. Within the filum and between the axons, very small deposits of lanthanum could be found demonstrating transfer of lanthanum from the interstitial to the periaxonal space (horizontal arrows)

Indeed, the labelling of the surface of fila olfactoria showed the leakage of tracer through the perineural sheath raising the question of the function of perineural TJs. Even the fila olfactoria were poorly labelled and not consistently empty of lanthanum staining (Fig. 10. F) suggesting that the TJs of OECs were able to hinder but not to obstruct completely the penetration of tracer into the fila olfactoria.

3.3. Rheological measurements

Rheological parameters like viscosity of the vehicle may influence the diffusion speed of the incorporated drug, in this way play important role in the drug release process. The flowcurves obtained in case of PhS, AE, HA and MA samples are shown on Fig. 11. Low shear stress values and a linear correlation between shear stress and shear rate were measured for both the physiological saline solution and the absorption enhancer containing system, typical for Newtonian flow behavior. The addition of the surface active agent in AE slightly increased the slope, reflecting the viscosity of the sample. The viscosity values of HA and MA vehicles containing sodium hyaluronate are two and three order of magnitude higher, respectively, than for PhS and AE. HA and MA solutions can be characterized by pseudoplastic flow behavior. The presence of the surfactant Cremophor RH40 in MA has decreased the viscosity of the vehicle to one tenth as compared to HA (Fig. 11.).

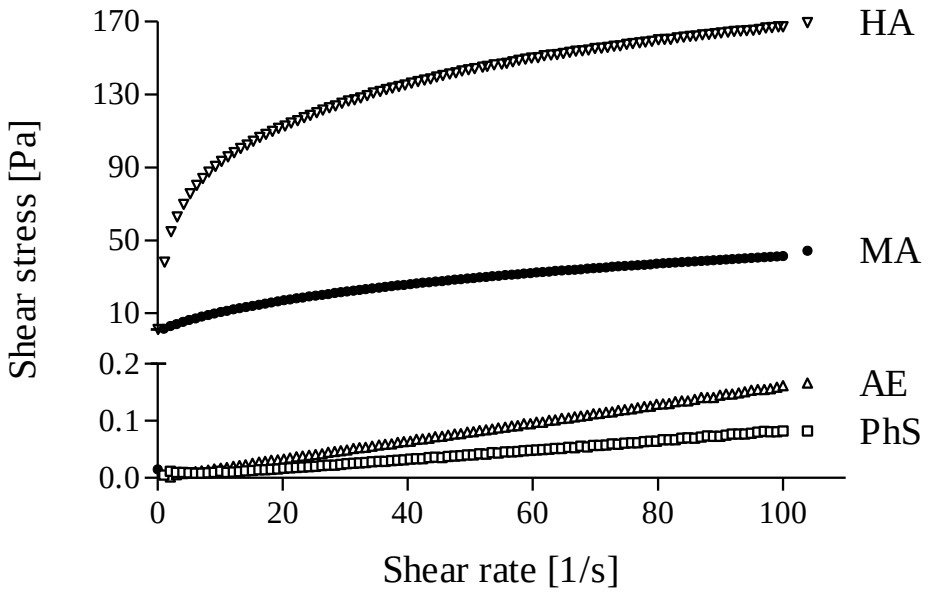

Fig. 11. Flowcurves of the physiological saline solution (PhS), the absorption enhancer Cremophor RH40 containing solution (AE), vehicle containing hyaluronan alone (5) HA, and vehicle containing mucoadhesive hyaluronan and absorption enhancer Cremophor RH40 (MA), n = 4.

3.4. *In vitro* drug release studies

The *in vitro* dissolution profiles of FD-4 from different vehicles are shown on Fig. 12. Carriers PhS and AE, not containing biopolymer, showed similar dissolution kinetics and profiles but in the case of vehicles containing the mucoadhesive hyaluronan, HA and MA, different dissolution profile could be detected (Fig. 12., Table 6.).

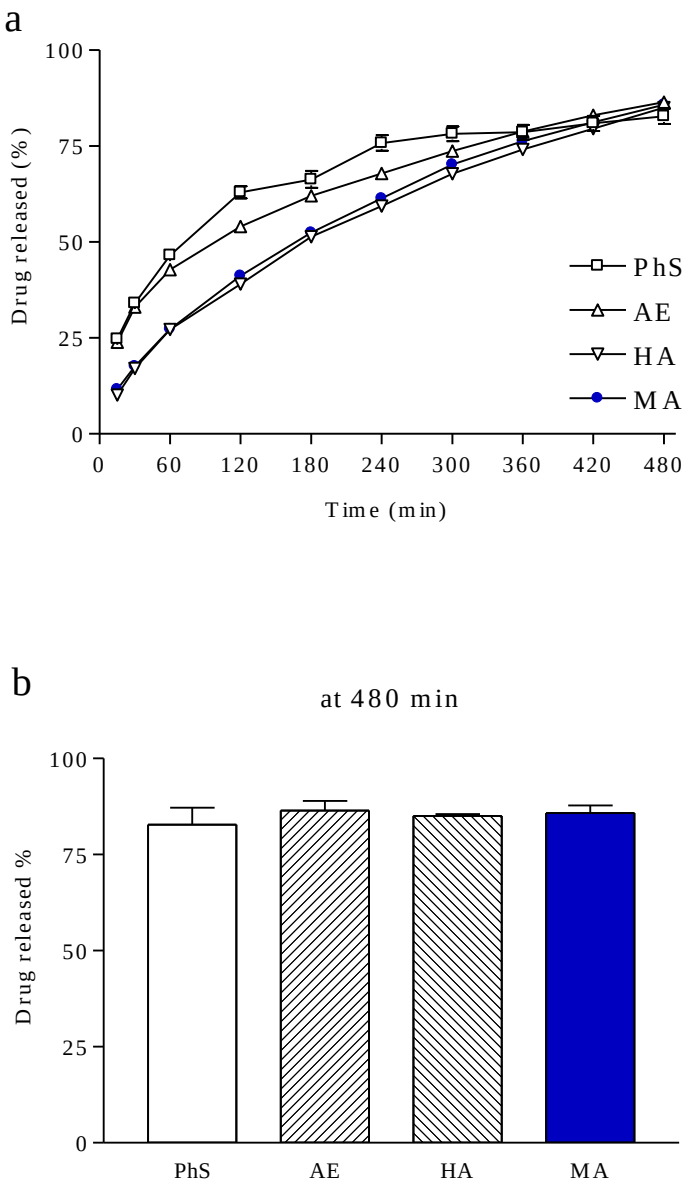

Fig. 12. Results of in vitro drug release studies. Dissolution profiles of FD-4 from different vehicles. (□) PhS, (Δ) AE, (▼) HA, (●) MA, (a). The amount of released FD-4 after 480 min of dissolution time (b). Data are presented as mean ± SEM, n = 12).

	PhS		AE		MA	
AE	f1=6.11	f2=66,85				
	similar					
MA	f1=19.96	f2=43.84	f1=15.38	f2=50.47		
	different		different			
HA	f1=22.36	f2=42.03	f1=18.02	f2=48.22	f1=3.13	F2=86.08
	different		different		similar	

Table 6. Comparison of dissolution profiles of different nasal vehicles. PhS, physiological saline solution; AE, vehicle containing absorption enhancer Cremophor RH40; HA, vehicle containing hyaluronan alone; MA, vehicle containing mucoadhesive hyaluronan and absorption enhancer Cremophor RH40.

The addition of hyaluronan slowed the release of FD-4 between 30-240 min. This effect can be related to the viscosity increasing effect of the polymer in agreement with the data of the rheological measurements (Fig. 11.). Despite the differences in the dissolution profiles, the same amount of FD-4 was released from the vehicles at 8 hours (Fig. 12.).

3.5. Quantitative investigation of FD-4 transport to the systemic circulation and to brain

3.5.1. Kinetics in plasma

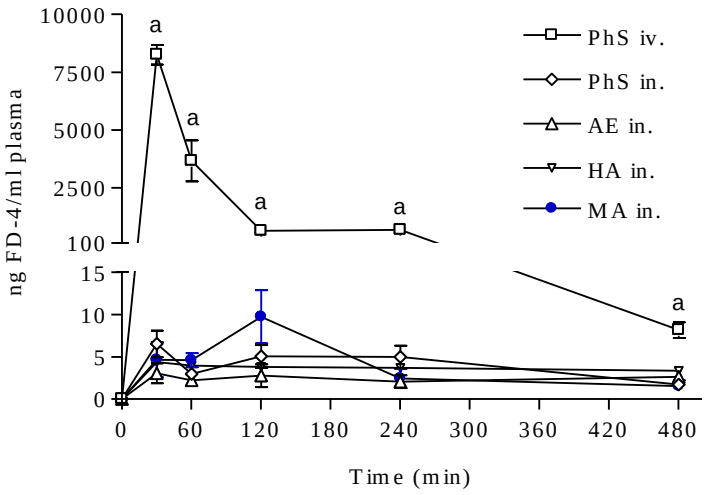

Fig 13. Plasma concentrations of FD-4, in vivo experiments. (□)PhS iv., (■) PhS in., (Δ) AE, (▼) HA, (●) MA in., [a]Concentrations measured in PhS iv. group were significantly ($P < 0.001$) higher at each time point than those in the other three groups. Plasma FD-4 levels did not differ significantly in the four intranasal groups at any time point. Data are presented as mean ± SEM, n = 4.

Intravenous injection of 4 mg FD-4 resulted in a high concentration, 8.25 μg/ml in the plasma at 30 min, which was still higher than 100 ng/ml 4 h after the injection (Fig. 13.). When FD-4 was administered nasally (for doses see Table 5.), three magnitude of order smaller plasma concentrations were measured. The highest plasma concentration, 20 ng/ml was measured in the MA group at 2 h timepoint. FD-4 levels in all groups were lower than 10 ng/ml at 8 h.

Vehicle	**c_{max} [ng FD-4/ml plasma] mean ± SD**	**t_{max} [min]**	**AUC mean ± SD**	**Relative BA mean ± SD**
PhS iv.	8253 ± 848	30	592411 ± 82638	1.00 ± 0.14
PhS in.	6.52 ± 3.16	30	1887 ± 730	0.32 ± 0.12
AE in.	3.04 ± 2.35	30	1129 ± 567	0.19 ± 0.10
HA in.	4.36 ± 0.53	30	1719 ± 79	0.29 ± 0.01
MA in.	9.73 ± 6.27	120	1847 ± 1060	0.31 ± 0.18

Table 7. Pharmacokinetic parameters in plasma. AUC, area under the concentration-versus-time curve; BA, bioavailability compared to the PhS iv. group; PhS, physiological saline solution; AE, vehicle containing absorption enhancer Cremophor RH40; HA, vehicle containing hyaluronan alone; MA, vehicle containing mucoadhesive hyaluronan and absorption enhancer Cremophor RH40; n = 4.

The plasma area under the concentration-versus-time curve (AUC) value of the intravenous injection group (PhS iv., Table 7.) is about 3-500 times higher than the AUC values in the nasal treatment groups, which do not differ from each other statistically. Taking into account the 100 times difference in the doses administered intravenously or nasally, the relative bioavailability (BA) of the FD4 given in nasal vehicles was about the 20-30% of the relative BA of the intravenous FD4.

3.5.2. Regional distribution in brain

The highest concentration of FD-4 was measured at 240 min in the olfactory bulb and in the frontal cortex in case of vehicle MA, containing both hyaluronate and Cremophor (Fig. 14.). In case of other carriers, smaller peaks can be observed and the corresponding t-max values are smaller. FD-4 concentrations in different brain regions are compared at 4 hours after the treatments (Fig. 15.). The highest values were obtained in case of MA mucoadhesive formulation.

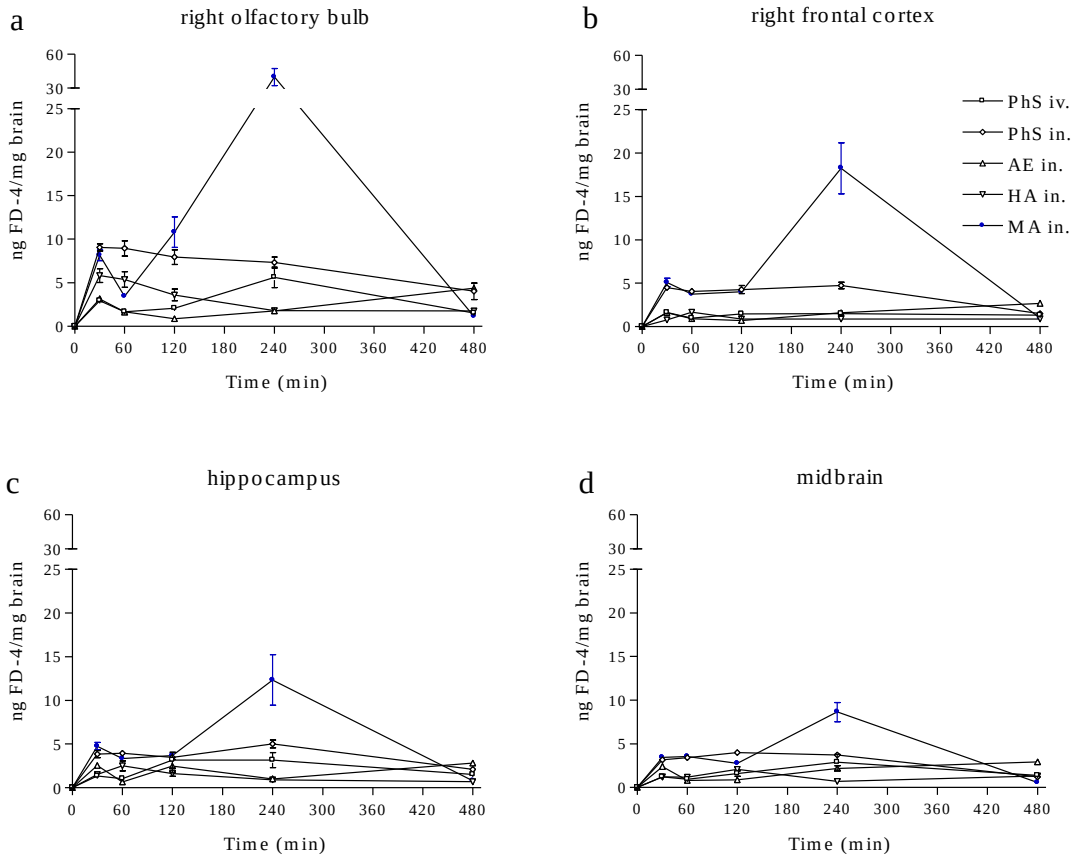

Fig. 14. Brain concentrations of FD-4, in vivo experiments. (□)PhS iv., (■) PhS in., (Δ) AE, (▼) HA, (●) MA in., (a) Olfactory bulb from the right side, (b) frontal cortex from the right side, (c) hippocampus, (d) midbrain. Data are presented as mean ± SEM, n = 4.

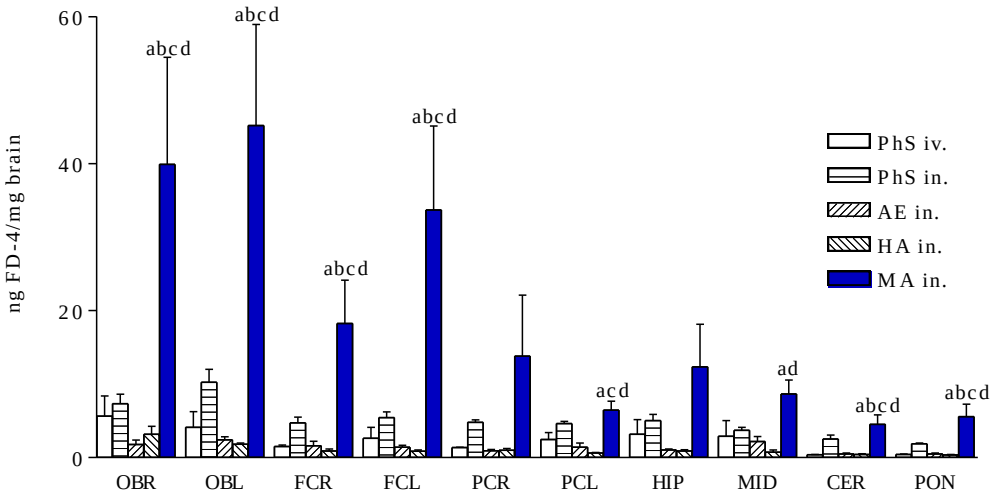

Fig. 15. FD-4 concentrations in different brain regions measured 240 min after different treatments (OBR: olfactory bulb from right side; OBL: olfactory bulb from the left side; FCR: frontal cortex from the right side; FCL: frontal cortex from the left side; PCR: parietal cortex from the right side; PCL: parietal cortex from the left side; HIP: hippocampus; MID: midbrain; CER: cerebellum; PON: pons). Statistically significant differences (P < 0.05) were detected in the MA group compared to the values measured in [a]PhS iv. group; [b]PhS in. group; [c]AE group; [d]HA group. Data are presented as mean ± SEM, n = 4.

Although the concentration of the FD-4 was decreased with the increasing distance from the nasal cavity, this vehicle significantly enhanced the nose to brain transport of the test molecule even in the pons and the cerebellum (Fig. 15).

The pharmacokinetic parameters in brain obtained after intranasal and intravenous administration of FD-4 are summarized in Table 8. The largest AUC value for all brain regions measured was obtained in case of the MA vehicle. To calculate the relative bioavailability the one hundred times higher dose of FD-4 applied intravenously was considered one. The highest relative BA value was 561.5 in case of MA formulation. Furthermore, the calculated relative bioavailability values were 2 orders of magnitude higher after the intranasal treatments as compared to the intravenous administration.

Vehicle	**c_{max} [ng FD-4/mg brain] mean ± SD**	**t_{max} [min]**	**AUC mean ± SD**	**Relative BA mean ± SD**
PhS iv.	1.72 ± 0.90	240	598 ± 178	1.0 ± 0.3
PhS in.	4.49 ± 0.14	120	1523 ± 97	254.7 ± 16.3
AE in.	2.07 ± 0.21	30	554 ± 83	92.7 ± 13.9
HA in.	1.39 ± 0.09	60	431 ± 52	72.2 ± 22.7
MA in.	15.21 ± 9.11	240	3358 ± 1713	561.5 ± 286.5

Table 8. Pharmacokinetic parameters in brain. AUC, area under the concentration-versus-time curve; BA, bioavailability compared to the PhS iv. group; PhS, physiological saline solution; AE, vehicle containing absorption enhancer Cremophor RH40; HA, vehicle containing hyaluronan alone; MA, vehicle containing mucoadhesive hyaluronan and absorption enhancer Cremophor RH40; n = 4.

AUC values in various brain regions were also determined and MA group had significantly higher AUC in the right olfactory bulb (OBR) and frontal cortex (FCR) than the other four treatment groups (OBR: PhS. iv. 1548 ± 865, PhS. in. 3197 ± 1066, AE 1096 ± 144, HA 1278 ±, 430, MA 8693 ± 5214, $P < 0.021$; FCR: PhS. iv. 653 ± 85, PhS. in. 1738 ± 136, AE 766 ± 129, HA 465 ± 112, MA 4087 ± 1067, $P < 0.009$).

In case of MA, nose to brain transport of the test molecule was also confirmed by fluorescent microscopy of frozen brain sections (data not shown). In agreement with the quantification data, high fluorescent intensity could be observed in the olfactory bulb and the frontal cortex, while no signal was detected in sections of control animals treated with solutions without FD-4 treated.

3.6. Electron microscopy

To test for toxic side-effects of the vehicles the olfactory system was investigated by electron microscopy (Fig. 16.). The olfactory epithelium, the epithelial cells and the apical microvilli of rats treated with MA solution did not show any pathological alteration in comparison with the untreated tissue (Fig. 16. A-B), indicating that the formulation has no acute toxic effect in the olfactory tissue. No morphological change could be observed in the olfactory fila within the lamina propria, showing again that the MA treatment did not induce any pathological effect on the ultrastructure of the sensory axons when compared with the nerve from the untreated tissue sample (Fig. 16. C-D).

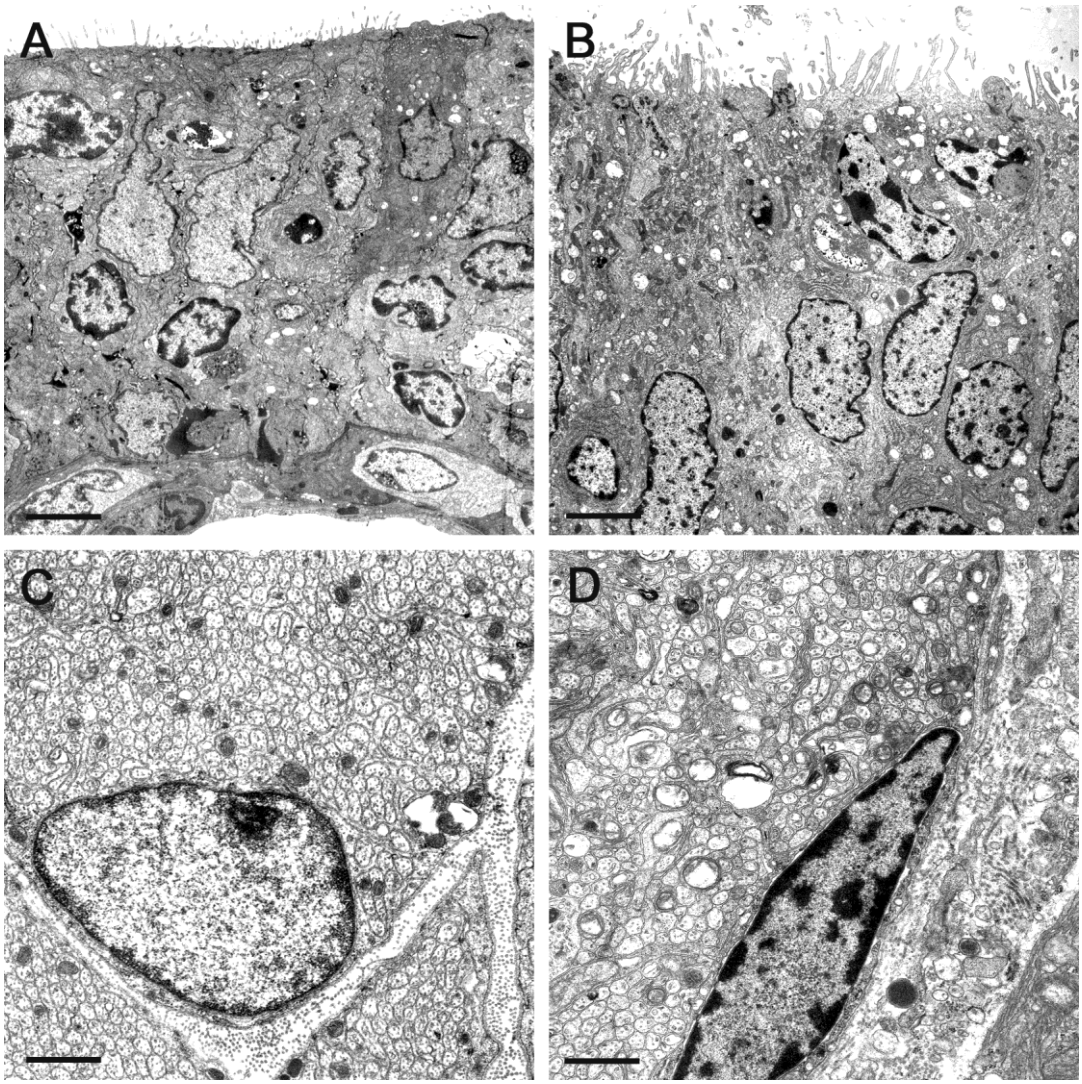

Fig. 16. Electron microscopical investigation of the olfactory system. A-B: *olfactory epithelium showing epithelial cells with apical microvilli;* C-D: *olfactory fila within the lamina propria underneath the olfactory epithelium. MA treatment (B, D) did not induce any pathological effect on the ultrastructure of the epithelium or sensory axons when compared with the untreated tissue (A, C). Bars in A-B: 5 μm, in C-D: 1 μm.*

4. DISCUSSION

Epithelial and endothelial barriers separate the organisms from the external environment and the body compartments from each other. The tight intercellular seals responsible for the effective separation were identified as zonula occludens or TJs by electron microscopy more than 50 years ago (for review see Gonzalez-Mariscal and Nava, 2005). In the last 25 years the discovery of the transmembrane proteins of TJs, like occludin, the claudin family and the signalling pathways regulating TJ functions resulted in a great advance in understanding how epithelial and endothelial barriers work and how this knowledge can be exploited in disease therapies, drug discovery and drug targeting.

The non-invasive delivery of hydrophilic drugs or large biopharmaceuticals to the systemic circulation or to specific organs protected by a barrier, like the CNS, is still a big challenge. Drug absorption or penetration across epithelial and endothelial barriers are restricted by several factors. Efflux transporters expressed at high levels in epithelia and the BBB prevent not only the flux of xenobiotics, but also drug molecules to reach their target (Abbott *et al*., 2006). Local metabolic barriers act as a second line of defence and specific enzymes are able to inactivate drugs, cleave proteins and peptides, or other biologically active compounds (El-Bacha and Minn, 1999). The third major cause is the presence of intercellular TJs that strictly limit the paracellular route. Several methods, molecules, and excipients have been investigated for the safe and reversible opening of these junctions to enhance drug absorption and penetration (Ward *et al*. 2000; Deli 2009).

In our studies we revealed by immunohistochemistry the TJ compositions of the major barriers of the olfactory system, and in subsequent experiments we designed and tested nasal vehicles to overcome these barriers and target a test molecule by the nasal pathway.

4.1. The morphological basis of nasal pathway

4.1.1. Junctional proteins in the olfactory system

The olfactory system possesses elaborate barriers (Fig. 4.). The three major barriers are the layers of epithelial cells connected by apical TJ complexes, endothelial cells of the blood vessels in the lamina propria and finally the OECs and perineural cells protecting the axons of the sensory olfactory neurons which are projected from the periphery to the CNS.

Epithelial cells

In our study epithelial cells showed strong staining for the classical cytoplasmic linker proteins of TJs ZO-1 and ZO-2. Interestingly, ZO-2 was also expressed in basal cells, which can reflect the nuclear transcription factor role of this protein. The presence of classical epithelial integral mebrane TJ proteins occludin, claudin-1 and -3 was not surprising in this barrier. The tight junction molecule claudin-5 is believed to be characteristic for endothelial cells (Morita *et al*., 1999). There has hitherto been one exception from the rule of endothelial expression of claudin-5, namely the expression by gastrointestinal epithelial cells (Rahner *et al.*, 2001). In this study we also described for the first time the presence of this molecule in olfactory epithelial cells. Surprisingly, we detected claudin-19, a claudin subtype present in Schwann-cells, in TJs between supporting cells and the dendrites of the sensory olfactory neurons.

Junctional protein	Epithelial cells	Endothelial cells	OECs
ZO-1	+++	+++	+++
ZO-2	++	-	-
Occludin	+++	+	+++
Claudin-1	+++	-	-
Claudin-3	+++	-	-
Claudin-5	+++	+	++
Claudin-19	++	-	-

Table 9. Summary of the immunohistochemical findings in the major barriers of the olfactory system.

Endothelial cells of the blood vessels in the lamina propria

Endothelial cells also expressed ZO-1 TJ protein, similarly to olfactory epithelial cells, but not ZO-2. As compared to both epithelial and OEC TJ, the immunostaining for occludin, and especially claudin-5 was much weaker, indicating a leaky barrier in these cells. Claudin-1, -3 and -19 was not found in this cell type.

Olfactory ensheating cells

To protect the olfactory axons from the full spectrum of blood-borne substances, many being neurotoxic, the TJs of the OECs are necessary to filter those compounds favourably for growing axons. OECs are similar in many ways to glial cells, for example, as we could demonstarte they express glial fibrillary acidic protein and also aquaporin 4. Glial barriers can express occludin, claudins and other TJ proteins. This prompted us to test the occurrence of claudin-1 in OEC TJs. However, the OECs turned out to be immunonegative for claudin-1, whereas the perineural cells and the apical tight junctions between supportive and sensory cells in the olfactory epithelium were found to be immunopositive for claudin-1 (Fig. 8. A, B). Similar to epithelial and endothelial cells, we found claudin-5 and in the OECs as well (Fig. 8. D). This finding may indicate that claudins are not expressed in a strictly cell-specific manner. The reason for testing claudin-19 in the olfactory system was the hypothesis of Wewetzer *et al.,* (2002) that all OECs are Schwann cells which develop their characteristic phenotype under the specific influence of the olfactory system. In this view, the absence of the Schwann cell-specific claudin-19 (Miyamoto *et al.,* 2005) reflects a suppression of this phenotype in the olfactory environment (Fig. 8. E).

In comparison to the other barriers of the olfactory system, the TJ protein pattern of OECs is similar to that of endothelial cells, and may consist of claudin-5, occludin and ZO-1. Our data summarized in Table 9. indicate, that the olfactory epithelial layer presents the most complex and possibly the most tight barrier from the point of view of drug targeting.

4.1.2. Permeability properties of the olfactory region

Dye study

Our study with fluorescein and Evan's blue dyes can be considered as the demonstration of Paul Ehrlich's classical experiments at the end of the 19th century. His observations on azo-dyes staining all tissues except the CNS indicated the presence of

some kind of barrier between the periphery and the CNS for the first time. Our findings shown in Fig. 9. indicate that the blood vessels of the lamina propria in both the respiratory and olfactory regions are highly permeable to the dyes in contrast to the vessels of the brain. These findings are in agreement with our data on the protein composition of the endothelial TJs of the olfactory mucosa described above.

Lanthanum study

In the present study, we demonstrated for the first time that the blood vessels of the lamina propria of the olfactory mucosa are leaky for perfused lanthanum nitrate as an accepted electron microscopical tracer. The OEC TJs form a barrier for lanthanum nitrate, which nevertheless is incomplete allowing a low amount of leakage from the interstitial to the periaxonal space (Fig. 10. F). This finding explains for the first time the morphological basis of the transport pathway between the nasal cavity and the CNS via the olfactory nerve (Fig. 5.).

Our data also indicate, that if a molecule is transported across the olfactory epithelium with the help of an appropriate nasal vehicle, the nasal pathway demonstrated for lanthanum can be used to reach the CNS.

4.2. Modulation of nasal targeting by formulating vehicles

Despite the potential of the nasal route, several factors limit the intranasal absorption of drugs (Illum, 2000; Illum, 2002; Illum, 2003). Mucociliary clearance, enzymatic activity, and the epithelium combined with the mucus layer constitute barriers to the nasal absorption especially of high-molecular-weight and hydrophilic drugs (Ugwoke *et al.*, 2005). Therefore, the use of absorption enhancers and the design of suitable dosage formulations, such as mucoadhesive delivery systems, are necessary to enhance the nasal bioavailability of these drugs (Pringels *et al*., 2008).

The main finding of our studies is that the combination of the surfactant Cremophor, as an absorption enhancer, and hyaluronic acid, as a viscosifying and bioadhesive polymer, could significantly increase the nose to brain transport of the test molecule FD-4, especially in the olfactory bulb and frontal cortex regions. These data are in accordance with the results of other authors (Thorne *et al*., 2004), who found similar brain distribution for insulin-like growth factor following intranasal administration. We hypothesize that peptides or peptide fragments in the size range of 1-4 kDa acting on

neuropeptide or hormon receptors in the nervous system, eg. peptides regulating appetite and body weight, could be targeted with the MA formulation for therapeutical purposes.

4.2.1. Surfactants as absorption enhancers

Surfactants are solubilizing excipients widely used in oral, injectable and nasal formulations (Strickley, 2004; Davis and Illum, 2003). Anionic, non-ionic synthetic surfactants and bile salts have been extensively studied to enhance transepithelial permeability for different marker molecules, peptides and drugs (Deli, 2009). Chremophor, a non-ionic surfactant has been only studied in a microemulsion vehicle for nasal administration until now (Zhang *et al.*, 2004).

In the present study the surfactant Cremophor RH40 was used as an absorption enhancer. Although surfactants, which are non-specific permeation enhancers, can improve the absorption of drugs by increasing their paracellular and transcellular transport via the modification of the cell membrane (Deli, 2009), no increase in the brain FD-4 levels was observed after application of AE vehicle compared to that of the PhS. A possible explanation can be the fast removal of both vehicle from the nasal cavity by the mucociliar activity. The higher test molecule levels in brain regions using MA formulation as compared to HA clearly indicates that Cremophor played an important role in enhancing the permeability for FD-4 of the main barrier of the olfactory system, namely the epithelium.

4.2.2. Role of mucoadhesion in nasal vehicles

Because of its favorable characteristics, natural biocompatibility, bioadhesiveness, and lack of immunogenicity, hyaluronic acid and its derivatives are used in ophthalmic, rheumatologic, tissue engineering, cosmetic and veterinary products (Liao *et al.*, 2005; Vercruysse and Prestwich, 1998). Although viscosity and mucoadhesion are key factors in nasal drug delivery (Ugwoke *et al.*, 2005), and hyaluronates have excellent mucoadhesive properties, only one study tested viscous sodium hyaluronate solutions in nasal absorption so far (Morimoto *et al.*, 1991). Hyaluronate solutions enhanced the nasal absorption of vasopressin in rats measured by a bioassay (Morimoto *et al.*, 1991). However, the vehicle contained no other components and the concentration of the peptides in the blood or in the CNS were not determined.

The incorporation of sodium hyaluronate alone as a viscosifying agent and mucoadhesive component into the vehicle HA in our experiments did not increase the amount of FD-4 transported to the brain in contrast to the combination of hyaluronan with Cremophor RH40, MA vehicle. The effect of MA is not related to elevation in plasma levels of FD-4, since FD-4, injected intravenously, resulted in a high AUC in plasma, and a low AUC in brain, due to the highly selective and strictly regulated transport processes of the BBB (Deli *et al*., 2005; Banks, 2005). The nasal formulations led to negligible plasma AUC, while the brain AUC of FD-4 in MA group exceeded that of the intravenously administered FD-4. This clearly indicates the circumvention of the BBB and a direct access to the CNS.

While the exact mechanism of this effect is not known, it is well documented, that mucoadhesive additives can reduce the mucociliary clearance rate, increase the residence time of the drug formulation in the nasal cavity, and hence prolong the period of contact with the nasal mucosa, which may improve drug absorption (Jansson *et al*., 2005; Ugwoke *et al*., 2005). Furthermore, some mucoadhesive polymer containing systems may directly change epithelial tight junctions and increase drug absorption and bioavailability (Lehr, 2000). The difference between the efficacy of nasal vehicles HA and MA may indicate, that optimal viscosity, supposed mucoadhesivity, longer residence time and absorption enhancement induced by the nonionic surfactant all contributed to the increased brain penetration of the test molecule.

Despite advances in nasal mucoadhesive drug delivery, the application of mucoadhesive agents in nasal vehicles may not work for all compounds (Ugwoke *et al*., 2005). In a recent paper a pectin formulation resulted in lower systemic absorption and lower brain uptake of a drug compared to a solution formulation in rats (Charlton *et al*., 2007). Differences in the experimental design, short vs. long treatment time intervals, presence vs. absence of absorption enhancer, different physico-chemical properties of the test molecule may explain the different results.

Toxicity is a major issue in the development of formulations for the nasal route (Ugwoke *et al*., 2005). It is very important to note, that in our study the vehicle containing sodium hyaluronate and Cremophor RH 40 did not induce tissue damage, epithelial or subepithelial toxicity, or ciliotoxicity (Fig. 16.). Our observations are in agreement with previous data, that acute and chronic toxicity tests in animals have shown Cremophors to be essentially non-toxic and non-irritant materials (Rowe *et al*., 2007). Hyaluronate solution did not affect the ciliary beat frequency of rabbit nasal mucosal membranes *in*

vitro (Morimoto *et al*., 2005), further supporting the non-toxic properties of this biomolecule. The excellent properties and safety profile of hyaluronic acid (Liao *et al*., 2005) could be better exploited for nasal drug delivery systems.

Conclusion

Combination of absorption enhancer materials and bioadhesive polymers, such as Cremophor RH 40 and sodium hyaluronate can potentially increase the delivery of drugs, including peptide size molecules, into the CNS via the olfactory pathway. Further experiments are in progress to test the efficacy of the MA system for targeting biologically active peptides to the brain.

5. SUMMARY

The non-invasive delivery of hydrophilic drugs or large biopharmaceuticals to the systemic circulation or to specific organs protected by a barrier, like the nervous system, is still a big challenge. The blood-brain barrier which separates the brain from the circulation prevents the brain penetration of the great majority of possible therapeutical molecules. Targeting drugs to brain tissue requires either transport through the blood-brain barrier, or utilization of alternative routes, like the nasal pathway. Due to the specific anatomical and physiological properties of the olfactory region, this pathway can be exploited as a direct route to the nervous system.

The three major barriers of the olfactory system are the epithelial cells, the endothelial cells of the blood vessels in the lamina propria and the olfactory ensheating cells which protect the axons of the olfactory neurons. We revealed the tight junction compositions of these barriers by immunohistochemistry. The tight junction protein pattern of rat endothelial and olfactory ensheating cells are similar and consist of claudin-5, occludin and ZO-1. The olfactory epithelial cells express also ZO-2, claudin-1, -3 and -19 in addition to the proteins found in endothelial cells, indicating that they represent the most complex and possibly the tightest barrier from the point of view of drug targeting. In accordance with these data we found that the blood vessels of the lamina propria of the olfactory mucosa are leaky for lanthanum nitrate, an electron microscopical tracer in contrast to the vessels of the brain. The olfactory ensheating cells form an incomplete barrier for lanthanum allowing leakage from the interstitial to the periaxonal space. This finding explains for the first time the morphological basis of the transport pathway between the nasal cavity and the nervous system via the olfactory nerve

We designed and tested nasal vehicles to overcome these barriers and target the test molecule fluorescein-labelled 4 kDa dextran by the nasal pathway to the brain in rats. From the four tested vehicle, the combination of the surfactant Cremophor, as an absorption enhancer, and hyaluronic acid, as a viscosifying and bioadhesive polymer, could significantly increase the nose to brain transport of the test molecule, especially in the olfactory bulb and frontal cortex regions. Morphological examination of the olfactory system revealed no toxicity of the vehicles. In conclusion, the nasal pathway has a potential for targeting therapeutical drugs to the central nervous system by circumventing the blood-brain barrier.

6. ACKNOWLEDGEMENTS

I am grateful to my supervisor and my mentor, Dr. Mária Deli for her scientific guidance, encouragement and support throughout my Ph.D. studies.

I would like to express my gratitude to my supervisor at the Department of Pharmaceutical Technology Prof. István Erős.

I thank Dr. László Siklós, head of the Laboratory of Molecular Neurobiology in the Institute of Biophysics, Biological Research Center, and Prof. Piroska Révész, head of the the Department of Pharmaceutical Technology for their support.

We are indebted to Prof. Hartwig Wolburg for the scientific cooperation between the research groups that made the electronmicroscopical and immunhistochemical studies of the olfactory system possible.

I am grateful to Dr. András Fehér, Lóránd Kiss, Dr. Anita Kurunczi, Dr. Levente Kürti, Dr. Péter Sipos, Andrea Tóth and Dr. Szilvia Veszelka for their inspiring help in the studies.

I would like to thank Ngo Thi Khue Dung for the excellent technical assistance.

I thank the members of the Group of Molecular Neurobiology their help and friendship.

Finally, I am especially thankful to Izabella Jámbor and my family for their love and untiring support during my studies.

The research was supported by grants from the Hungarian Research Fund (OTKA T37834, T37956, M036252), the National Office for Research and Technology (RET 08/2004, GVOP-KMA-52), and the Foundation of Gedeon Richter.

7. REFERENCES

Abbott, N.J., Ronnback, L., Hannson, E., 2006. Astrocyte-endothelial interactions at the blood–brain barrier. *Nat. Rev. Neurosci*. 7: 41–53.

Banks, W.A., 2005. Blood-brain barrier transport of cytokines: a mechanism for neuropathology. *Curr. Pharm. Des*. 11: 973-84.

Begley, D.J., 2004. ABC transporters and the blood-brain barrier. *Curr Pharm Des*. 10: 1295-1312.

Behl, C.L., Pimplaskar HK, Sileno AP, deMeireles J, Romeo, V.D., 1998 Effects of physicochemical properties and other factors on systemic nasal drug delivery. *Adv. Drug Deliv. Rev.* 29: 89–116.

Bodor N, Buchwald P., 2002. Barriers to remember: brain-targeting chemical delivery systems and Alzheimer's disease. *Drug Discov Today*. 7: 766-774.

Bonferoni, M.C., Giunchedi, P., Scalia, S., Rossi, S., Sandri, G., Caramella, C., 2006. Chitosan gels for the vaginal delivery of lactic acid: relevance of formulation parameters to mucoadhesion and release mechanisms. *AAPS Pharm. Sci. Tech*. 7: 104.

Charlton, S.T., Davis, S.S., Illum, L., 2007. Evaluation of effect of ephedrine on the transport of drugs from the nasal cavity to the systemic circulation and the central nervous system. *J. Drug Target*. 15: 370-377.

Cho, K.Y., Chung, T.W., Kim, B.C., Kim, M.K., Lee, J.H., Wee, W.R., Cho, C.S., 2003. Release of ciprofloxacin from poloxamer-graft-hyaluronic acid hydrogels *in vitro*. *Int. J. Pharm*. 260: 83–91.

Costantino, H.R., Illum, L., Brandt, G., Johnson, P.H., Quaya, S.C., 2007. Intranasal delivery: Physicochemical and therapeutic aspects. *Int. J. Pharm*. 337: 1–24.

Davis, S.S., Illum, L., 2003. Absorption enhancers for nasal drug delivery. *Clin. Pharmacokinet*. 42: 1107-1128.

Deli, M.A., 2009. Potential use of tight junction modulators to reversibly open membranous barriers and improve drug delivery. *Biochim. Biophys. Acta* 1788: 892-910

Deli, M.A., Ábrahám, C.S., Kataoka, Y., Niwa, M., 2005. Permeability studies on *in vitro* blood–brain barrier models: physiology, pathology, and pharmacology. *Cell. Mol. Neurobiol*. 25: 59–127.

Egleton, R.D., Davis, T.P., 2005. Development of neuropeptide drugs that cross the blood-brain barrier. *NeuroRx* 2: 44-53.

El-Bacha, R.S., Minn, A., 1999. Drug metabolizing enzymes in cerebrovascular endothelial cells afford a metabolic protection to the brain. *Cell. Mol. Biol. (Noisy-le-grand)*. 45: 15-23.

Enerson BE, Drewes LR., 2006. The rat blood-brain barrier transcriptome. *J. Cereb. Blood Flow Metab.* 26: 959-973.

Garcia-Garcia, E., Andrieux, E.K., Gilb, S., Couvreur, P., 2005. Colloidal carriers and blood–brain barrier (BBB) translocation: A way to deliver drugs to the brain? *Int. J. Pharm.* 298: 274–292.

González-Mariscal, L., Nava, P., 2005. Tight junctions, from tight intercellular seals to sophisticated protein complexes involved in drug delivery, pathogens interaction and cell proliferation. *Adv. Drug. Deliv. Rev.* 57: 811-814.

Guidance for Industry, Dissolution Testing of Immediate Release Solid Oral Dosage Forms. US Food and Drug Administration, Rockville, MD, 1997. http://www.fda.gov/cder/Guidance/1713bp1.pdf

Illum, L., 2000. Transport of drugs from the nasal cavity to the central nervous system. *Eur. J. Pharm. Sci.* 11: 1–18.

Illum, L., 2002. Nasal drug delivery: new developments and strategies. *Drug Discov. Today* 7: 1184-1189.

Illum, L., 2003. Nasal drug delivery-possibilities, problems and solutions. *J. Control. Release* 87: 187–198.

Illum, L., 2004. Is nose-to-brain transport of drugs in man a reality? *J. Pharm. Pharmacol*. 56: 3-17.

Jansson, B., Hägerström H, Fransén N, Edsman K, Björk E, 2005 The influence of gellan gum on the transfer of fluorescein dextran across rat nasal epithelium *in vivo*. *Eur. J. Pharm. Biopharm*. 59: 557-564.

Jiang, D., Liang, J., Noble, P.W., 2007. Hyaluron in tissue injury and repair. *Annu. Rev. Cell Dev. Biol*. 23: 435-461.

Khafagy, El-S., Morishita, M., Onuki, Y., Takayama, K., 2007. Current challenges in non-invasive insulin delivery systems: A comparative review. *Adv. Drug Deliv. Rev*. 59: 1521-1546.

Krizbai I.A., Deli M.A., 2003. Signalling pathways regulating the tight junction permeability in the blood-brain barrier. *Cell. Mol. Biol. (Noisy-le-grand).* 49: 23-31.

Lehr, C.M., 2000. Lectin-mediated drug delivery: The second generation of bioadhesives. *J. Control. Release* 65: 19–29.

Li, Y., Field, P.M., Raisman, G., 2005 Olfactory ensheathing cells and olfactory nerve fibroblasts maintain continuous open channels for regrowth of olfactory nerve fibres. *Glia* 52: 245–251

Liao, Y.H., Jones, S.A., Forbes, B., Martin, G.P., Brown, M.B., 2005. Hyaluronan: pharmaceutical characterization and drug delivery. *Drug Deliv*.12: 327-342.

Liebner, S., Fischmann, A., Rascher, G., DuVner, F., Grote, E.-H., Kalbacher, H., Wolburg, H., 2000. Claudin-1 expression and tight junction morphology are altered in blood vessels of human glioblastoma multiforme. *Acta Neuropathol*. 100: 323–331

Lim, S.T., Martin, G.P., Berry, D.J., Brown, M.B., 2000. Preparation and evaluation of the *in vitro* drug release properties and mucoadhesion of novel microspheres of hyaluronic acid and chitosan. *J. Control. Release* 66: 281–292.

Ludwig, A., 2005. The use of mucoadhesive polymers in ocular drug delivery. *Adv. Drug Deliv. Rev*. 57: 1595– 1639.

Miller, G., 2002 Drug targeting. Breaking down barriers. *Science.* 297: 1116-1118.

Miyamoto, T., Morita, K., Takemoto, D., Takeuchi, K., Kitano, Y., Miyakawa, T., Nakayama, K., Okamura, Y., Sasaki, H., Miyachi, Y., Furuse, M., Tsukita, S., 2005. Tight junctions in Schwann cells of peripheral myelinated axons: a lesson from claudin-19-deficient mice. *J. Cell Biol*. 169: 527–538

Morimoto, K., Yamaguchi, H., Iwakura, Y., Marisaka, K., Ohashi, Y., Nakai, Y., 1991. Effect of viscous hialuronate-sodium on the nasal absorption of vasopressin and an analogue. *Pharm. Res.* 8: 471-474.

Morita, K., Sasaki, H., Furuse, M., Tsukita, S., 1999. Endothelial claudin: claudin-5/TMVCF constitutes tight junction strands in endothelial cells. *J. Cell Biol.* 147: 185–194

Muldoon, L.L., Soussain, C., Jahnke, K., Johanson, C., Siegal, T., Smith, Q.R., Hall, W.A., Hynynen K, Senter PD, Peereboom DM, Neuwelt EA, 2007. Chemotherapy delivery issues in central nervous system malignancy: a reality check, *J. Clin. Oncol*. 25: 2295–2305.

Narang, A.S., Delmarre, D., Gao, D., 2007. Stable drug encapsulation in micelles and microemulsions. *Int. J. Pharm.* 345: 9-25.

Neuwelt, E.A., Maravilla, K.R., Frenkel, E.P., Rapoport, S.I., Hill, S.A., Barnett, P.A., 1979. Osmotic blood-brain barrier disruption. *J. Clin. Invest*. 64: 684 –688.

O'Hara, T., Dunne, A., Butler, J., Devane, J., 1998. A review of methods used to compare dissolution profile data. *Pharm. Sci. Technol*. Today 1: 214-223.

Okuyama, S., 1997 The first attempt at radioisotopic evaluation of the integrity of the nose-brain barrier. *Life Sci.* 60: 1881-1884

Pardridge, W.M., 2002. Drug and gene targeting to brain with molecular Trojan horses, Nat. *Rev. Drug Discov*. 1: 131–139.

Pardridge, W.M., 2005. The blood-brain barrier: bottleneck in brain drug development. *NeuroRx. 2:* 3-14.

Pouton, C.W., 2006. Formulation of poorly water-soluble drugs for oral administration: Physicochemical and physiological issues and the lipid formulation classification system. *Eur. J. Pharm. Sci*. 29: 278–287.

Pringels, E., Vervaet, C., Verbeeck, R., Foreman, P., Remon, J.P., 2008. The addition of calcium ions to starch/Carbopol((R)) mixtures enhances the nasal bioavailability of insulin. *Eur. J. Pharm. Biopharm*. 68: 201-206.

Rahner, C., Mitic, L.L., Anderson, J.M., 2001. Heterogeneity in expression and subcellular localization of claudins 2, 3, 4, and 5 in the rat liver, pancreas, and gut. *Gastroeneterology* 120: 411–422

Rash, J.E., Davidson, K.G.V., Kamasawa, N., Yasumura, T., Kawasama, M., Zhang, C., Michaels, R., Restrepo, D., Ottersen, O.P., Olson, C.O., Nagy, J.I., 2005. Ultrastructural localization of connexins (Cx36, Cx43, Cx45), glutamate receptors and aquaporin-4 in rodent olfactory mucosa, olfactory nerve and olfactory bulb. *J. Neurocytol.* 34: 307–341

Regea, B.D., Kaob, J.P.Y., Polli, J.E., 2002. Effects of nonionic surfactants on membrane transporters in Caco-2 cell monolayers. *Eur. J. Pharm. Sci*. 16: 237–246.

Rowe, R.C., Sheskey, P.J., Owen, S.C. (Eds.), 2005, Handbook of Pharmaceutical Excipients. *Pharmaceutical Press, London*, 572-579.

Schnyder, A., Huwyler, J., 2005. Drug transport to brain with targeted liposomes, *NeuroRx 2:* 99-107.

Shah, V.P., Tsong, Y., Sathe, P., Liu, J.-P., 1998. *In vitro* dissolution profile comparison – statistics and analysis of the similarity factor. *Pharm. Res*. 15: 889-896.

Somogyi, G., Nishitani, S., Nomi, D., Buchwald, P., Prokai, L., Bodor, N., 1998. Targeted drug delivery to the brain via phosphonate derivatives I. Design, synthesis and evaluation of an anionic chemical delivery system for testosterone. *Int. J. Pharm*. 166: 15–26.

Strickley, R.G., 2004. Solubilizing excipients in oral and injectable formulations. *Pharm. Res.* 21: 201-230.

Takano, M., Yumoto, R., Murakami, T., 2006. Expression and function of efflux drug transporters in the intestine. *Pharmacol. Therapeut*. 109: 137–161.

Temsamani, J., Scherrmann, J.M., Rees, A.R., Kaczorek, M., 2000. Brain drug delivery technologies: novel approaches for transporting therapeutics. *Pharm. Sci. Technol. Today* 3: 155-162.

Thorne, R.G., Pronk, G.J., Padmanabhan, V., Frey, W.H., 2004. Delivery of insulin-like growth factor-I to the rat brain and spinal cord along olfactory and trigeminal pathways following intranasal administration. *Neuroscience* 127: 481–496.

Ugwoke, M.I., Agu, R.U., Verbeke, N., Kinget, R., 2005. Nasal mucoadhesive drug delivery: background, applications, trends and future perspectives. *Adv. Drug Deliv. Rev*. 57: 1640-1665.

Vercruysse, K.P., Prestwich, G.D., 1998 Hyaluronate derivatives in drug delivery. *Crit. Rev. Ther. Drug Carrier Syst.* 15: 513-555.

Ward, P.D., Tippin, T.K., Thakker, D.R., 2000. Enhancing paracellular permeability by modulating epithelial tight junctions. *Pharm. Sci. Technol. Today* 3: 346-358.

Wewetzer, K., Verdu, E., Angelov, D.N., Navarro, X., 2002. Olfactory ensheathing glia and Schwann cells: two of a kind? *Cell Tissue Res*. 309: 337–45

Zhang, Q., Jiang, X., Jiang, W., Lu, W., Su, L., Shi, Z., 2004. Preparation of nimodipine-loaded microemulsion for intranasal delivery and evaluation on the targeting efficiency to the brain. *Int. J. Pharm*. 275, 85–96.